Regulation of lipid dysmetabolism and neuroinflammation linked with Alzheimer's disease through modulation of Dgat2

Archana Yadav[1], Xiaosen Ouyang[1], Morgan Barkley[1], John C Watson[1], Kishore Madamanchi[1], Josh Kramer[1], Jianhua Zhang[1, 2], Girish Melkani[1, 2]

[1]Department of Pathology, Division of Molecular and Cellular Pathology, Heersink School of Medicine, University of Alabama at Birmingham, Birmingham, AL 35294, USA. [2] UAB Nathan Shock Center, Birmingham, AL 35294

[2]Corresponding Address: Department of Pathology, Division of Molecular and Cellular Pathology, School of Medicine, University of Alabama at Birmingham, AL 35294, USA. Tel.: 1-205-996-0591; Fax: 1-205-934-7447; E-mail: girishmelkani@uabmc.edu (GCM)

Abstract

Alzheimer's disease (AD) is a progressive neurodegenerative disorder marked by amyloid-β (Aβ) plaque accumulation, cognitive decline, lipid dysregulation, and neuroinflammation. While mutations in the Amyloid Precursor Protein (APP) and Aβ42 accumulation contribute to AD, the mechanisms linking Aβ to lipid metabolism and neuroinflammation remain unclear. Using Drosophila models, we show that App^{NLG} and Aβ42 expression causes locomotor deficits, disrupted sleep, memory impairments, lipid accumulation, synaptic loss, and neuroinflammation. Similar lipid and inflammatory changes are observed in the App^{NLG-F} knock-in mouse model, reinforcing their role in AD pathogenesis. We identify diacylglycerol O-acyltransferase 2 (Dgat2), a key lipid metabolism enzyme, as a modulator of AD phenotypes. In Drosophila and mouse AD models, Dgat2 levels and its transcription factors are altered. Dgat2 knockdown in Drosophila reduced lipid accumulation, restored synaptic integrity, improved locomotor and cognitive function, and mitigated neuroinflammation. Additionally, Dgat2 modulation improved sleep and circadian rhythms. In App^{NLG-F} mice, Dgat2 inhibition decreased neuroinflammation and reduced AD risk gene expression. These findings highlight the intricate link between amyloid pathology, lipid dysregulation, and neuroinflammation, suggesting that targeting Dgat2 may offer a novel therapeutic approach for AD. Conserved lipid homeostasis mechanisms across species provide valuable translational insights.

Keywords: Alzheimer's disease (AD); diacylglycerol O-acyltransferase 2; lipid metabolism; amyloid precursor protein, amyloid β; neuroinflammation, sleep, circadian rhythm, drosophila, mouse models.

Abbreviations

ABCA1: ATP-Binding Cassette Transporter A1

Aβ: Amyloid β

ACC: Acetyl-CoA carboxylase

AD: Alzheimer's disease

ApoE: Apolipoprotein E

APP: Amyloid precursor protein

BMP: Bis-phosphates

Dgat2: Diacylglycerol O-acyltransferase 2

Dgat2 KD: Diacylglycerol O-acyltransferase 2 knockdown

Dgat2 OE: Diacylglycerol O-acyltransferase 2 overexpression

EcR: Ecdysone receptor

Eip75B: Ecdysone induced protein 75B

FAS: Fatty acid synthase

GWAS: Genome-wide association studies

Nfat: Nuclear factor of activated T-cells

PICALM: Phosphatidylinositol-binding clathrin assembly protein

PSEN1: Presenilin1

PSEN2: Presenilin2

Srebp: Sterol regulatory element binding protein

TF: transcription factor

TREM2: Triggering receptor expressed on myeloid cells 2

TRF: Time-restricted feeding

WT: Wildtype

Introduction

Alzheimer's disease (AD) is a progressive neurodegenerative disorder that primarily affects older adults and is the leading cause of dementia worldwide[1,2]. While the exact causes of AD are still not fully understood, genetic mutations play a significant role, especially in early-onset familial forms of the disease. Three rare single-gene variants, Amyloid Precursor Protein (APP), Presenilin1 (PSEN1), and Presenilin2 (PSEN2) are known to be responsible for these familial cases. APP encodes the amyloid-β precursor protein, which, when cleaved by enzymes such as β-secretase and γ-secretase, generates amyloid-β (Aβ). These amyloid-β peptides aggregate into plaques, a pathological feature found in the brains of AD patients. Despite decades of research into the pathophysiology of AD, the precise molecular mechanisms driving the disease remain unclear, and there is still no effective and safe treatment to slow or halt its progression[3-5]. In addition to plaques, neuroinflammation plays a critical role in the development of AD, with elevated pro-inflammatory cytokines, reduced anti-inflammatory responses, and heightened glial cell reactivity. Lipids, particularly fatty acids, and their derivatives, have long been recognized for their immunomodulatory effects, capable of triggering either pro-inflammatory or anti-inflammatory responses depending on the lipid class and the target cell[6,7].

As one of the critical aspects of AD pathogenesis, altered lipid profiles and lipid accumulation have been found in both animal models and postmortem human AD brains[8,9]. Several lipid-related genes have been identified as genetic risk factors for AD, including Apolipoprotein E (ApoE), ABCA1 (ATP-Binding Cassette Transporter A1), PICALM (Phosphatidylinositol-binding clathrin assembly protein), and TREM2 (Triggering receptor expressed on myeloid cells 2)[10, 11]. Notably, the ApoE ε4 allele is a well-established genetic risk factor for late-onset AD, with ApoE playing a crucial role in lipid transport and neuronal integrity[12]. The upregulation of enzymes like fatty acid synthase (FAS) and acetyl-CoA carboxylase (ACC) in AD models suggests disrupted lipid synthesis, with palmitic acid (C16) accumulation near amyloid plaques, highlighting lipid pathways as potential therapeutic targets in AD[13-15]. In addition to neurons, astrocytes are a diverse group of neural cells that primarily degrade fatty acids in the brain. Their metabolic role in AD and neurodegeneration is beginning to be understood, with recent studies suggesting that impaired astrocytic fatty acid degradation may contribute to lipid dysregulation in the

brain[15]. This dysfunction in astrocytes could represent a key mechanism driving the pathophysiology of AD. Human Eph14 knock-in in astrocytes shifts metabolism towards increased glucose usage and reduced fatty acid β-oxidation, leading to lipid accumulation[16, 17]. Both microglia and astrocytes express enzymes for β-oxidation, with fatty acid metabolism influencing microglial phenotype and inflammation. Inhibition of β-oxidation in macrophages and microglia exacerbates inflammation while enhancing fatty acid oxidation reduces lipid-induced inflammation. Activation of mitochondrial function in microglia helps alleviate neuroinflammation and promotes amyloid-β clearance[18-20]. In transgenic mice expressing a mutant APP, there was an increase in *Aβ42* deposits in the brain along with elevated plasma cholesterol levels, further supporting the involvement of disrupted lipid metabolism in AD pathogenesis[21, 22]. Elevated levels of lysophospholipids and ceramides have been detected around Aβ plaques in the human AD brain. Similarly, in $App^{NLG\text{-}F}$ knock-in mice, an age-dependent increase in lysophospholipids and bis-phosphates have been observed near Aβ plaques[23]. Despite these findings, the precise role of lipid metabolism in AD pathology remains underexplored. Understanding how lipid dysregulation contributes to AD could open new avenues for therapeutic intervention.

One of the key enzymes involved in lipid metabolism is diacylglycerol O-acyltransferase 2 (Dgat2), which catalyzes the final step in triglyceride synthesis[24]. Interestingly, Dgat2 has been implicated in both lipid metabolism and the regulation of circadian rhythms, suggesting that its role extends beyond simple lipid storage and may influence the timing of metabolic processes[25-27]. Dgat2 expression in *Drosophila* and other animals is influenced by a variety of transcription factors, including Ecdysone-induced protein 75B (Eip75B), Ecdysone receptor (EcR), Nuclear factor of activated T-cells (Nfat) and Sterol regulatory element binding protein (Srebp), some of which are linked to lipid metabolism[28-31]. While the transcriptional regulation of Dgat2 is less well-established compared to other metabolic genes regulated by SREBP, recent research indicates that Dgat2 inhibition reduces lipogenesis by blocking SREBP-1 cleavage and lowering Srebf1 gene expression in the liver[32, 33]. In AD models and postmortem human AD brains, Dgat2 is upregulated, suggesting a potential link between Dgat2 activity and AD pathology[34]. However, the precise mechanisms by which Dgat2 contributes to AD, particularly in the context of APP mutation and lipid dysmetabolism, remain clear.

Circadian rhythms, which regulate various physiological processes, including sleep, cognition and metabolism. In AD, circadian rhythms are often disrupted, leading to sleep disturbances and cognitive decline. Interestingly, circadian rhythms influence lipid metabolism, and disruptions in circadian timing can lead to metabolic dysfunction, including altered lipid storage and degradation[35-37]. Furthermore, our previous work has shown that modulating lipid metabolism function in *Drosophila* melanogaster (commonly known as fruit fly), a model organism for studying human diseases[25, 38]. We also observed that ApoE induces lipid accumulation in the brain, with ApoE4 uniquely causing this accumulation independently of Dgat2, while ApoE2 and ApoE3 require Dgat2 for lipid buildup[25]. These findings highlight the importance of lipid metabolism in AD and suggest that targeting lipid metabolism pathways could mitigate ApoE-related metabolic dysfunction in AD. These findings suggest a strong connection between lipid metabolism and AD pathology[25].

In this study, we use *Drosophila* and *mouse* models of AD to investigate the effect of APP and *Aβ42* with and without Dgat2 modulation (*Drosophila*) and with Dgat2 Inhibitor (Mouse) on AD-related phenotypes. Panneuronal, glial, and mushroom body-specific expression of *UAS-App^{NLG}, UAS-Aβ42* induced lipid dysmetabolism and neurodegeneration in flies. Our innovative finding in *Drosophila* models of *App^{NLG}* mutations and *Aβ42* reveal progressive locomotor impairments, sleep disturbances, memory deficits, lipid accumulation, and neuroinflammation. Knockdown of Dgat2, improved inflammatory and metabolic gene expression, enhanced locomotor function, and improved sleep activity and circadian rhythms, suggesting the potential benefits of modulating lipid metabolism through Dgat2. For the mouse study, we use *App^{NLG-F}* knock-in mice with elevated Aβ pathogenic levels due to the combined effects of three mutations associated with familial AD[39]. These mice develop amyloid plaques, neuroinflammation, synaptic loss, and cognitive deficits, providing a robust model to study the progression of AD. In this model we have shown that lipid accumulation and neuroinflammation occur. Dgat2 inhibition decreased neuroinflammation responses, and reduced expression of AD risk genes. These findings suggest that targeting Dgat2 may offer a potential therapeutic strategy for AD, emphasizing the conserved impact of lipid metabolism across species.

Material and Methods

Drosophila models

Flies were maintained on a standard regular diet: agar 11 g/L, active dry yeast 30 g/L, yellow cornmeal 55 g/L, molasses 72 mL/L, 10% nipagen 8 mL/L, and propionic acid 6 mL/L. Flies were housed at 25 °C, 50% humidity in a 12-h light/12-h dark (LD) cycle and changed to new food every 3-4 days[27, 40-42]. We used the following driver's lines from Bloomington Drosophila Stock Center (BDSC) Elav(X)-Gal4 (BL#458) for panneuronal expression[43], GLaz-Gal4 (BL#8765) for glial expression[44] and OK107-Gal4 (BL#854) for mushroom bodies[45]. We used the following UAS lines UAS-APP^{NLG} (APP human APP carrying the familial Alzheimer's Swedish K670N, M671L, and Arctic E693G mutations, BL#33794) and UAS-Aβ42 (BL#33769). As previously described, we have also used UAS-hDgat2 (BL#84854), UAS-Dgat2 RNAi (BL#107788), and UAS-GFP (BL#5431)[25, 27, 46]. Moreover, we have used the following RNAi stocks to knock down potential transcription factors of Dgat2. UAS-Eip75B (BL#26717), EcR (BL#58286), UAS-Nfat (BL#51422), UAS-Vri (BL#25989), and UAS-Srebp (BL #25975). As recently reported, we used the UAS-Gal4 system to drive tissue-specific expression or knockdown of Dgat2 in specific brain regions[25]. Flies with *Elav > DGAT2* or *Elav > Dgat2 RNAi* (with a balancer25) were crossed with *UAS-AppNLG*, *UAS-Aβ42*, or control constructs to investigate their effects[47].In addition to each UAS line driven under different drivers, the driver and UAS lines alone and GFP overexpression serve as controls as previously reported[25, 27, 46.] Briefly, the progeny of the above-mentioned crossed flies will be collected at eclosion, separated by sex, held at a density of 25 flies/vial, and maintained on the diet mentioned above. As indicated in the results section, experiments were performed on 3-week (early middle age) and 7-week-old (old age) male or female flies as previously reported[25, 27, 46].

Mice

All mouse breeding, procedures, and experiments were approved by the Institute Animal Care and Use Committee (IACUC) at the University of Alabama at Birmingham. Mice were maintained in the Laboratory Animal Shared Resource with controlled air, light, and temperature conditions and fed ad libitum and free access to water. The *App^{NLG-F}* mice

carry three familial AD-associated mutations in the APP gene: Swedish mutation *(NL),* which enhances total *Aβ* production; Iberian mutation *(F),* which increases the *Aβ42/ Aβ40* ratio; and Arctic mutation *(G),* which promotes Aβ aggregation by facilitating oligomerization and reducing proteolytic degradation[39, 48]. *App*$^{NLG\text{-}F}$ and WT (controls) mice, maintained in C57BL/6J background, were euthanized by cervical dislocation, at the ages of 4 months (n=3) and 15 months (n=3). Half of the brain was used for immunohistochemistry and half of the cortex was used for RNA analyses.

Dgat2 Inhibitor

To investigate whether Dgat2 contributes to AD-related phenotypes, we used PF-06424439 (MedChemExpress, CAS No#1469284-78-3), a Dgat2 noncompetitive, slowly reversible inhibitor with an IC_{50} of 14nM. We injected PF-06424439 intraperitoneally at 0, 10, and 30 mg/kg to 3 each male 12 months old *App*$^{NLG\text{-}F}$ mice daily for 5 consecutive days. The euthanizing method was the same as above.

Drosophila olfactory aversion training to test memory

Flies were trained using the olfactory aversive conditioning method as previously described[8, 49]. Approximately 30-40 groups of flies were used for each genotype. Each genotype was exposed to two neutral odors (3-octanol and 4-methylcyclohexanol) prepared as a 1/10 dilution in mineral oil. A current of 100-V and 90-Hz was used as a shock reinforcer. Memory conditioning was performed using a T maze apparatus (CelExplorer Labs). The olfactory aversive conditioning consists of three phases: naïve, training, and testing. During the naïve phase, flies are exposed to both odors for 3 minutes and 30 seconds to determine their odor preference based on the odor presented in each odor chamber. A single training round consists of exposing flies to odor paired with electrical shock for 2 minutes, followed by 2 minutes of exposure to odor paired without shock. Depending on the fly's naïve odor preference, electrical shocking will be paired with their preferred odor. After three training rounds, flies are given 10 minutes to recover. During the testing phase, flies are given 3 minutes and 30 seconds to choose between odor chambers. Once time has expired, T maze chambers are sealed, and the number of flies in each chamber is scored. A performance index (PI) was calculated based on flies' avoidance of odor paired with electrical shock. To confirm these findings,

we conducted a sensory acuity test based on avoidance index calculations, as previously described[50].

***Drosophila* locomotion assay**

To evaluate the panneuronal and glial-specific expression of APP mutation and the impact of Dgat2 KD and OE on locomotor capability, we have developed a new 3D-printer-based device to analyze locomotive performance, using machine learning methods (manuscript under preparation). Briefly, the device holds 12 vials and features a Raspberry Pi Camera aimed precisely at them, which is connected to a Raspberry Pi 4B and a monitor. A custom Python script developed in our lab is running on the Raspberry Pi, controlling both the camera and an attached motor system. Video was recorded after tapping the device and the Faster RCNN deep learning model was used to detect vial boundaries in the video. The flies' climbing behavior was recorded on video for later analysis. Followed by python analysis processes video frames for fly detection and detection across time for average climbing were plotted.

***Drosophila* sleep circadian activity**

Sleep-wake and circadian activity behavior was recorded using the Drosophila Activity Monitor (DAM, TriKinetics Inc MA, USA) system in a 12L: 12D cycle at 25°C[51]. We used 3-week and 7-week-old male and female progeny of Elav-Gal4 and GLaz-Gal4 with control lines of each of the four genes *(w^{1118}, GFP, App^{NLG}, Aβ42*). We have also used Dgat2 transcription factors KD genes, *Eip75b, EcR, Nfat, Vri, and Srebp)*. Drosophila activity (or wake) is measured by infra-red beam crosses in the DAM system. Data was analyzed using Clock Lab and R Studio. Custom R scripts and methodology used with R Studio can be found at https://github.com/jameswalkerlab/Gill_et.al. Non-parametric One-way ANOVA with multiple comparisons Kruskal Wallis test for DAM system data was performed using Graph Pad Prism. Drosophila sleep was defined by a period of at least 5 minutes of inactivity, demonstrated by zero beam breaks recorded. Average sleep per 24 hours (Zeitgeber Time (ZT) is a standardized way of measuring time within a circadian cycle, where ZT0 represents the beginning of the light phase and ZT12 marks the start of the dark phase), of each genotype, was calculated. Five days were used for analysis of 3-week-old flies, and 3 days were used for 7-week-old fly experiments due to decreased viability in older flies. Sleep fragmentation was defined by the number of 1-minute wakes

for 24 hours. Sleep bouts were quantified by counting the number of periods of sleep as defined above. Sleep bout length was quantified by measuring the length of each sleep bout. Data for daytime sleep is from ZT0 to ZT12, and nighttime sleep is from ZT12-ZT24.

Histological analysis of *Drosophila* brain samples

The impact of APP mutation and *Aβ42*, with and without Dgat2 modulation, on lipid and synapsin alternations was investigated as previously described[41, 52.] Briefly, fly heads were excised under a dissecting microscope, then fixed in 4% paraformaldehyde (PFA) in phosphate-buffered saline (PBS) for 15 minutes at room temperature with mild agitation. The heads were washed three times for 10 minutes in 1× PBS. After the final wash, heads were transferred to a 10% sucrose in PBS solution, ensuring full saturation overnight. They were next arranged in a mold using optimal cutting temperature (OCT) compound. Once frozen in place, the samples were sectioned at 20μm using a Leica CM3050 S cryostat and transferred onto warmed glass slides (Fisher #15-188-48). After a 30-minute drying period and application of a hydrophobic border, slides were washed three times for 5 minutes with 1× PBS to remove the dried OCT. The slides were then blocked with 3% BSA in TBS solution for 30 minutes and incubated overnight at 4°C or for 1 hour at room temperature with primary synapsin antibody (1:250, UI Developmental Studies Hybridoma Bank #3C11) in 3% BSA in TBS. After incubation, slides were washed three times for 5 minutes with PBS and incubated for 1 hour at room temperature with an AlexaFluor-750 anti-mouse fluorescent secondary antibody (1:500, Thermo Fisher # A-21037) and lipid (1:100, Lipid Spot488, Biotinum #70065). Finally, slides were washed three times for 5 minutes with 1× PBS and mounted with Antifade Mounting Medium with DAPI (0.9μg/ml, VECTASHIELD Vibrance H-1800). After overnight setting, multichannel fluorescence images were captured using an Olympus BX63 fluorescence microscope and analyzed with CellSens software at 10× magnification to view one section of the head per image.

The DAPI channel was used to define regions of interest (ROIs), as it clearly distinguishes between anatomical sub-regions in the head. Two distinct ROIs were drawn around both whole head tissue and all brain lobes. For each ROI, both the object size and mean object area were collected from the 488nm channel, and the mean pixel intensity was collected from the 750nm channel. Multiple sections were imaged for each

fly, and the average fluorescent intensity as well as average object count, and area were compiled across sections to determine the overall lipid accumulation value per group. The 488 (lipid) channel was thresholded to reduce the background signal and the minimum object size for detection was set to 20 pixels. The 750 (synapsin) channels remained unthresholded to retain integrity during intensity comparison between individual subjects as well as conditions. All thresholding values and any background filters were applied in batches across all images before data collection. Selection of multiple sections (n≥3) per fly and multiple flies within each condition (n≥3) ensured all areas of the head and brain are equally weighted during comparison.

Mice brain staining, and image quantification

One brain hemisphere was placed in 4% paraformaldehyde overnight at 4ºC followed by sucrose incubation. The brain sample was frozen in OCT blocks and stored at -80ºC. 10µm tissue was cryosectioned. Nile red (Sigma: N3013) and LipidSpot™ 488 (Biotium NC1669425) were performed for Lipid Droplet Staining following the company's instructions. Gfap (Dako: Z0334, 1:20,000) or Iba1/AIF-1 (Cell Signaling Technology 17198S: 1:100) were paired with secondary Alexa fluor 488 (Invitrogen cat# A11008, 1:1,000). Hoechst (Fisher PI62249) was used as a nuclear stain. Images were acquired using the Keyence BZ-X810 microscope and ImageJ was used for image analysis.

Real-time quantitative PCR in *Drosophila* and mouse brain samples

As previously reported[25], the heads of 3-week-old and 7-week-old flies were isolated and rapidly frozen. RNA extraction was performed using the Zymo Research Quick-RNA Microprep Kit (catalog R1051, Zymo Research, Irvine, CA, USA), which included on-column DNase I digestion. Quantitative PCR was conducted using the Sso Advanced Universal SYBR Green supermix from Bio-Rad, employing the BIO-RAD CFX Opus Real-Time PCR System. Expression levels were standardized using the 60s ribosomal protein (Rpl11) as a reference three biological replicates were used with 8-10 flies each. Primers for qPCR are listed below:

Upd1-F: CAGCGCACGTGAAATAGCAT; Upd1-R: CGAGTCCTGAGGTAAGGGGA;
Upd2-F: AGCGTCGTGATGCCATTCA; Upd2-R: GCGATACGGATTGACATCGAA;
Upd3-F: ATCCCCTGAAGCACCTACAGA; Upd3-R: CAGTCCAGATGCGTACTGCTG;
Dome-F: CTCACGTCTCGACTGGGAAC; Dome-R: AGAATGGTGCTTGTCAGGCA;

Hop-F: CACCACCAACACCAATTC; Hop-R: GGAACGTCGTTTGGCCTTCT;
Stat92e-F: CCTCGGTATGGTCACACCC; Stat92e-R: TGCCAAACTCATTGAGGGACT;
Eiger-F: GATGGTCTGGATTCCATTGC; Eiger-R: TAGTCTGCGCCAACATCATC;
Imd-F: TCAGCGACCCAAACTACAATTC; Imd-R: TTGTCTGGACGTTACTGAGAGT;
Reaper-F: TGGCATTCTACATACCCGATCA;
Reaper-R: CCAGGAATCTCCACTGTGACT;
Hid-F: CACCGACCAAGTGCTATACG; Hid-R: GGCGGATACTGGAAGATTTGC;
Desat2-F: GTCGGCTACCCCTAGTCTGG; Desat2-F: TCGCCCTTGTGAATATGGAGT;
Amph-F: TCAAGTCCTCATTCCGCTCAA; Amph-R: CGGTTGCGCTTCTCTACTTTT;
Abca3-F: GCTCCTCGTTCTAGTCCGC; Abca3-R: TTGCAGCAGATTGAGGTCTGT;
P130CAS-F: GGTCTTCCGAAGGCTTCTAAC;
P130CAS-R: GCCACGCTCTTGAGTGTCT;
Eph-F: TTGGCACATGCAGATCAGGTT; Eph-R: TGGTGTTTGGGCTTGAGGTC;
Ank-F: AGCTGCAATGCAAACGGTCT; Ank-R: CCCCTTCTTAGCAACTCGCA;
Rho5-F: GGAAACGGAATGGCGGCTAA; Rho5-R: ATTGCGGAGTTGACTGCGATT;
Nlaz-F: ACGCCAACTACAGTCTCATAGA; Nlaz-R: CGAGGGTTGTCCGGTGAATC;
Eip75b-F: ATGCAACAGAGCACCCAGAAT;
Eip75b-R: CATGGAGTAGGAGGGGCAATC;
Nfat-F: AAAGACAGCCGGGTAAGGGAT; Nfat-R: CAGGAACCATTTTGCCAGGAC;
EcR-F: GTCCCGGAGAACCAATGTG; EcR-R: GGCGAAGTGGTCATTTTGTCC;
Srebp-F: ACCAACAGCCACCATACATCA; Srebp-R: AGACAAAGCTACTGCCCAGAG;
Dgat2-F: ATCCGTTGTGGATGGCAATG;
Dgat2-R: GGGAAAGTAATCACGATAGTGGC;
Rpl11-F: CGATCTGGGCATCAAGTACGA; Rpl11-R: TTGCGCTTCCTGTGGTTCAC;
Results are presented as $2^{-\Delta\Delta Ct}$ values normalized to the expression of Rpl11 and. All reactions were performed in triplicate.

Mouse RNA extraction was performed by using RNeasy Plus Mini Kit (Qiagen, Cat#: 74134) from isolated mouse cortex samples. cDNA synthesis was performed using a High-Capacity cDNA Reverse Transcription Kit (Thermo Fisher Scientific, Cat#: 4368814). Primers for mouse qPCR are listed below:

Bin1-F: TTCGGACCTATCTGGCTTCTG; Bin1-R: CCTCCTGAAGACACTCACTCA;

Abca7-F: AATTACACCTATCGACGGAGACA; Abca7-R: TGACGGACAGCCACTAGGA;
Cass4-F: CCAGGGCACTCTACGACAAC; Cass4-R: GCACATTTTGTTCCACGATGG;
Epha1-F: AGGAAGTCACTCTAATGGACACA;
Epha1-R: CCTCACTCCACCCAGTCTCT;
Ank1-F: GGAGCGTCACCCAATGTCTC; Ank1-R: GGCCACTTCTGTATGCCCTG;
Rhbdf2-F: GCCCACACCGTATCTGTTCTG;
Rhbdf2-R: GATGCCAGTTTTGTCGCTTGC;
Apoe-F: GACCCAGCAAATACGCCTG; Apoe-R: CATGTCTTCCACTATTGGCTCG;
Nr1d1-F: ACTTCCCACCATCACCTACTG; Nr1d1-R: GGGGAGCTATCATCACTGAGA;
Nfat5-F: GAGGGGTGTGGATTGGAATCT;
Nfat5-R: CTGGTGCTCATGTTACTGAAGTT;
Nr1h2-F: GCCTGGGAATGGTTCTCCTC; Nr1h2-R: AGATGACCACGATGTAGGCAG;
Srebf1-F: TGACCCGGCTATTCCGTGA; Srebf1-R: CTGGGCTGAGCAATACAGTTC;
Picalm-F: CTGACGGACCGAATCACCG; Picalm-R: GTGGCCTTGCATACTGTCTTAG;
Eda-F: AGTGCTCAATGACTGGTCTCG; Eda-R: CGCTGCGGGGATGTAGTTTA;
Stat5b-F: CGATGCCCTTCACCAGATG; Stat5b-R: AGCTGGGTGGCCTTAATGTTC;
Ptprq-F: ATTTCTGCCACAACCTACAGC;
Ptprq-R: GGAGGGGTATTCCATGAAAGGAG;
Jak2-F: TTGTGGTATTACGCCTGTGTATC; Jak2-R: ATGCCTGGTTGACTCGTCTAT;
Ripk1-F: AGAAGAAGGGAACTATTCGCTGG;
Ripk1-R: CATCTATCTGGGTCTTTAGCACG;
Scd1-F: TTCTTGCGATACACTCTGGTGC; Scd1-R: CGGGATTGAATGTTCTTGTCGT;
Dgat2-F: TTCCTGGCATAAGGCCCTATT; Dgat2-R: CCTCCAGACATCAGGTACTCG;
Results are presented as $2^{-\Delta\Delta Ct}$ values normalized to the expression of β-actin.

Statistical analysis

Significance climbing ability were determined using two-way ANOVA with multiple comparisons done with Uncorrected Fisher's LSD test. Significance was based on chi-square test for olfactory aversion training, and the difference between fly decisions, and flies avoiding shock odor were analyzed with one-way ANOVA with Tukey’s multiple comparisons test. Lipid droplet size and density differences and synaptic loss were performed by one-way ANOVA with Dunnett's multiple comparisons test for *Drosophila.*

Relative mean intensity of lipid, Gfap and Iba1 were measured using two-way ANOVA with Tukey's multiple comparisons test for young and old mouse samples, one-way ANOVA with Tukey's multiple comparisons test for Dgat2 inhibitor. For sleep activity analysis, differences between samples were determined using Non-parametric one-way ANOVA with multiple comparisons done with the Kruskal Wallis test. Quantitative PCR analyses were made using one-way ANOVA with Tukey's multiple comparisons test were performed for *Drosophila* samples and two-way ANOVA with multiple comparisons done with Uncorrected Fisher's LSD test was performed for young/ old mouse samples. One-way ANOVA with Tukey's multiple comparisons test were performed for *mouse* samples using Dgat2 inhibitor. Bar graphs show mean ± SD. All statistical analyses were performed with Graph Pad Prism 10. Differences were considered to be significant at values of $*p < 0.05$; $**p < 0.01$; $***\ p < 0.001$.

Results

A brief outline of our study is shown in **Fig.1a**, to reveal the involvement of beta amyloid in AD progression using *Drosophila* and mouse models. As indicated in the method section, using *Drosophila* models, we have tested the impact of *UAS-App^{NLG}, and UAS-Aβ42* upon their expression in panneuronal (Elav), glial (GLaz), and mushroom body (Ok-107) drivers. The outline also demonstrated the use of *Dgat2 knock-down (KD),* and over-expression (OE) of human Dagt2 (hDgat2). Geotaxis assays assessed locomotor performance, and sleep-circadian activity was conducted using the DAM system to investigate the impact of APP mutation and Dgat2 modulation. As previously reported olfactory aversion training was performed to test memory upon expression of APP mutants and Dgat2 modulations. Gene expression analyses of lipid metabolism, neuro-inflammation, and AD risk genes were conducted. All experiments included appropriate controls (W^{1118} and GFP) at two different ages **(Fig. 1a).**

In the *App^{NLG-F}* mouse model of AD, along with wild type control mice, we examined lipid accumulation and glial activation by immunofluorescence. Additionally, qPCR was

performed to assess the expression of genes involved in lipid metabolism, neuroinflammation, and AD risks. The effects of a Dgat2 inhibitor on lipid accumulation, neuroinflammation, and AD risk gene expression were also evaluated **(Fig. 1a).**

Panneuronal, glial or mushroom-body specific expression of A*pp^{NLG} and Aβ42* led to compromised locomotor and/or cognitive performance

As shown in **Fig.1b**, distinct differences in compromised locomotor performance were observed upon expression of *App^{NLG}* and A*β42,* with more pronounced impairments in Aβ42 expressing flies and more modest effects in *App^{NLG}* females, compared to age-matched control in 3-week-old flies. Similar trends were seen in male flies with Elav-*Aβ42,* whereas male flies expressing *App^{NLG}* construct showed no significant changes in the climbing ability regardless of the driver used**.** These results suggest that the geotaxis phenotype is driver-specific and impacts locomotor performances prominently in females than male, whether through panneuronal or glial expression **(Fig.1b).** To investigate cognitive performance, we subjected wild type, *App^{NLG}* and *Aβ42* flies to olfactory aversive conditioning, which test their ability to associate odors with reinforcers **(Fig.1c-e)**. 3-week-old female flies expressing *App^{NLG}* and *Aβ42* driven by Elav and GLaz resulted in significantly impaired cognitive performance **(Fig. 1c, d, left panels).** Expression of these AD-linked genes in the mushroom body using the OK-107 driver led to even greater deficits in olfactory aversion training **(Fig. 1e, left panel).**

Additionally, we performed two olfactory aversion analyses measuring both odor (measured by the odor avoidance index) and shock acuity (measured by electric shock avoidance index) **(Fig 1 d-e, middle and right panels respectively).** Both approaches revealed similar conclusion. These findings indicate that the expression of AD-linked genes in the mushroom bodies has a more profound impact on memory compared to panneuronal and glial expression, highlighting the critical role of these brain regions in olfactory learning. This suggests that different brain regions contribute to cognitive dysfunction in AD models, offering new insights into the mechanisms underlying AD-related memory impairment.

Compromised circadian activity in flies with panneuronal and glial-specific expression of *Aβ42 and in* aged glial-specific expression of *App^{NLG}*

Compromised circadian activity was observed in flies with panneuronal and glial-specific expression of *Aβ42* and in aged glial-specific expression of *App^{NLG}*. Various sleep and circadian parameters, including day, night, and total sleep duration, circadian activity, sleep quality, fragmentation, bout length, and bout number, were analyzed in 3 and 7-week-old male flies with panneuronal and glial-specific expression of *App^{NLG}* and *Aβ42* **(Fig. 2 and Extended Data Fig. 1a-c, Fig. 2a-c, Fig. 3a-f).** These data were compared to controls to evaluate the impact of AD mutations on sleep behavior. As shown in **Fig. 2a,** neuronal-specific expression of *Aβ42* led to a significant increase in overall sleep time compared to controls in 3wk old flies, particularly during the night **(Fig. 2a).** The increased sleep was accompanied by higher sleep fragmentation, most notably during the nighttime **(Fig. 2c).** Although a similar trend was observed with *App^{NLG}* but changes were not statistically significant. These findings suggest that while the panneuronal-specific expression of *Aβ42* led to more sleep, but the quality of sleep was compromised due to higher sleep fragmentation **(Fig. 2a-c)**

As shown in **Fig. 2d and Extended Data Fig. 2a-c,** flies with glial-specific expression App^{NLG} and *Aβ42* genes exhibited significantly increased sleep in *Aβ42,* which was primarily due to extended sleep during the nighttime, as sleep profile showing sleep minutes/ hours for 24 hours **(Fig. 2e).** This increase in sleep was associated with higher sleep fragmentation during the nighttime in *App^{NLG}* and total sleep fragmentation in both *App^{NLG}* and *Aβ42* **(Fig. 2f),** suggesting that while the total sleep duration increased, the quality of sleep was negatively impacted. The increased sleep duration was thus accompanied by poor sleep quality, as indicated by elevated fragmentation.

Additionally, panneuronal expression of *Aβ42* led to a decrease in the total number of sleep bouts, especially at night, suggesting fewer, longer sleep periods **(Extended Data Fig. 1b-c).** In contrast, glial-specific expression of *App^{NLG}* and *Aβ42* caused an increase in the number of sleep bouts during the day, with longer day bout lengths, indicating a distinct pattern of sleep fragmentation **(Extended Data Fig. 2a-c).** In 7-week-old flies, sleep disturbances persisted and worsened, indicating that these disruptions are

not transient but progressively worsen with age (**Extended Data Fig. 3a-f).** These findings suggest that sleep disturbances are a lasting feature of AD models.

Panneuronal and glial-specific expression of *App^{NLG}* and *Aβ42* led to increased lipid accumulation and reduced synapsin levels

Our study revealed a significant increase in lipid accumulation, as indicated by green positive cells (Lipid spot) in both the *App^{NLG} and Aβ42* flies, compared to their respective control groups at 3-week **(Fig. 3a-f).** Notably, panneuronal-driven *App^{NLG} and Aβ42* flies exhibited more prominent lipid accumulation than glial-driven models, suggesting that lipid dysregulation is a prominent feature of *App^{NLG} and Aβ42* models, potentially contributing to the pathophysiology of AD. Additionally, synapsin expression was markedly reduced in both *App^{NLG} and Aβ42* flies. Synapsin staining intensity was significantly lower in these flies compared to controls, indicating impaired synaptic function **(Fig. 3d, f).** This reduction was observed in both panneuronal and glial-driven *App^{NLG} and Aβ42* flies. At 7-week, lipid accumulation remained elevated in both the *App^{NLG} and Aβ42* flies in both panneuronal and glial drivers. While synapsin level remain unchanged in panneuronal driven flies but were reduced in glial-driven *App^{NLG}* model, suggesting a stabilization or compensatory adaptation in synaptic function (**Extended Data Fig.4a-f**). These findings indicate an early phase of synaptic damage followed by a potential plateau in synaptic decline, with persistent lipid and amyloid changes pointing to ongoing pathophysiological processes. Overall, the results suggest that lipid dysregulation and synapsin impairment are strongly linked in AD progression, with the *App^{NLG}* model potentially reflecting more closely the synaptic dysfunction observed in AD, which may contribute to cognitive and sleep disturbances.

***App^{NLG-F}* mice exhibit age dependent increase of lipid accumulation and glial activation**

We performed immunostaining in the cortex (Ctx) region of the *App^{NLG-F}* mice to assess the level of lipid spot staining and Gfap immunoreactivity respectively at different age (young and old mice). In 15-month-old *App^{NLG-F}* mice, we observed a notable increase in

lipid accumulation, as indicated by enhanced lipid spot intensity **(Fig.3g, i)**. Additionally, Gfap level, which marks astrocytic activation, was significantly higher in 15-month-old *App*$^{NLG-F}$ compared to age-matched wild-type (WT) controls **(Fig. 3h, j).**

We also examined Nile red and Dgat2 staining in the Ctx **(Extended Data Fig. 4g-j).** Nile red staining was significantly increased in old *App*$^{NLG-F}$ mice, while Dgat2 staining showed no change in intensity, although Dgat2 aggregates were observed in the hippocampal CA1 region and cerebellum **(Extended Data Fig. 5a-d).** Furthermore, we evaluated Adrp, a protein that binds lipid droplets, and found no significant changes in its levels in the cortex or hippocampal (CA1) regions **(Extended Data Fig. 6a-d).** Immunostaining for Gfap and Iba1 in the CA1 region **(Extended Data Fig. 7a-d)** revealed a significant increase in Gfap-positive cells in 15-month-old *App*$^{NLG-F}$ mice. Iba1-positive cells, marking microglial activation, were also significantly higher in both young and old *App*$^{NLG-F}$ mice compared to WT controls. Notably, aging did not affect Iba1 expression in WT mice, but a dramatic increase in Iba1 was observed in 15-month-old *App*$^{NLG-F}$ mice, both in the CA1 region **(Extended Data Fig. 7a-b)** and in the cortex (**Fig. 4a, b)**. These findings suggest that aging in *App*$^{NLG-F}$ mice is associated with increased lipid accumulation, astrocytic activation, and microglial changes, consistent with age-related neuroinflammation in AD models.

Age-dependent increase in AD risk gene expression in the *App*$^{NLG-F}$ mouse model

In the *App*$^{NLG-F}$ mice, we observed a significant age-dependent increase in Iba1, which is a marker of microglia activation **(Fig. 4a, b and Extended Data Fig.7a-d).** This rise in Iba1 suggests that microglia become more activated with age, possibly due to the amyloid plaque's accumulation in the brain. Microglia initially respond to plaques and other damage by becoming activated to clear harmful debris, but chronic activation over time can lead to neuroinflammation. This persistent activation can reduce the efficiency of microglial function, contributing to neuronal damage and the progression of neurodegenerative diseases like Alzheimer's. To explore this further, we examined the expression of key inflammatory genes. Notably, protein tyrosine phosphatase receptor type Q (Ptprq), showed a mark upregulation with age **(Fig. 4c)**, supporting the idea of chronic, age-related inflammation. However, other inflammatory markers, such as Janus

kinase2 (Jak2), ectodysplasin (Eda), and signal transducer and activator of transcription 5B (Stat5b) did not show significant change, suggesting a more selective inflammatory response. In addition to neuroinflammation, we assessed the expression of metabolic genes. Notably, Srebf1 expression was significantly increased with age, while no significant changes were observed in other metabolic genes, such as stearoyl-CoA desaturase (Scd) and Dgat2, indicating a possible alteration in lipid metabolism (**Fig. 4d)**.

Further investigation of AD risk genes revealed an age-dependent increase in the expression of Bridging integrator 1 (Bin1) and ATP binding cassette subfamily A member 7 (Abca7), both of which are involved in amyloid processing and lipid transport. This upregulation suggests a potential link to increased amyloid burden or alterations in lipid metabolism, both of which are key features of Alzheimer's pathology. Additionally, we observed elevated expression of rhomboid family-like 2 (Rhbdf2) and Apoe genes that are also associated with neuroinflammation and lipid homeostasis **(Fig. 4e)**. Taken together, the increased expression of Iba1, Ptprq, and several AD risk genes with age highlights the progressive activation of neuroinflammatory pathways and suggests that lipid metabolism and inflammatory responses are central contributors to the neurodegenerative processes in the *App^{NLG-F}* mouse model. This growing evidence reinforces the idea that neuroinflammation and the dysregulation of Alzheimer's-related pathways progressively exacerbate pathology as the mice age.

App^{NLG} and *Aβ42*-linked locomotor and cognitive dysfunction was improved with Dgat2 KD and aggravated with Dgat2 OE

We assessed geotaxis, and cognitive function, in 3-week-old flies to investigate the effects of *App^{NLG}* and *Aβ42* in relation to the panneuronal expression of *Dgat2KD* and OE. First, a geotaxis assay was used to assess locomotor performance. At 3 weeks of age, significant differences in locomotor performance were observed between flies expressing the *App^{NLG}* gene and their respective controls **(Fig.5a).** Male flies with panneuronal *Dgat2 KD* displayed improved climbing ability when expressing *App^{NLG} or Aβ42, w*hile female flies show similar trends, though less significantly. In contrast, flies with Dgat2 OE did not show any improvement in climbing ability compared to controls

(Fig. 5a). These results suggest that Dgat2 KD may protect locomotor performance, while Dgat2 OE may worsen it.

We next evaluated if cognitive performance was altered in *Dgat KD* and OE. Male flies expressing *GFP, Aβ42,* and App^{NLG} exhibited memory impairment, which was rescued when Dgat2 was KD **(Fig. 5b, left panel)**. However, memory impairment was not rescued in flies expressing Dgat2 OE **(Fig. 5c, left panel).** Further analysis of odor avoidance using the performance index **(Fig. 1)** supported these findings, reinforcing the idea that Dgat2 manipulation affects both locomotion and cognition **(Fig. 5b, c, middle and right panel).** In conclusion, our results suggest that Dgat2 KD has a protective effect, improving both locomotor and cognitive function, whereas Dgat2 OE exacerbates deficits in these areas.

Dgat2 KD leads to the restoration of sleep activity and reduced sleep fragmentation linked with the expression of App^{NLG} and *Aβ42*

We assessed sleep activity in Elav-driven Dgat2 KD and OE flies at both 3 and 7 weeks of age to explore the potential links between sleep, cognitive function, and memory performance which were observed in earlier tests in App^{NLG} and *Aβ42*. At 3 weeks of age, both Dgat2 KD and Dgat2 OE flies expressing *Aβ42* exhibited a more prominent increase in total sleep, including daytime and nighttime sleep compared to App^{NLG}. Both groups (Dgat2 KD and OE) showed reduced sleep fragmentation, indicating a more continuous sleep pattern. Notably, there were no significant differences in sleep patterns between Dgat2 KD and Dgat2 OE flies at 3-week age **(Fig. 5d, e).** These suggest that, Dgat2 manipulation at 3 weeks does not drastically disrupt sleep, rather both conditions resulted in increased total sleep and reduced sleep fragmentation, indicating a relatively similar pattern. Further investigation revealed changes in sleep activity in the App^{NLG} and *Aβ42* models, such as fewer sleep bouts and increased bout length, particularly in flies with Elav-driven *Dgat2 KD.* Similar trends were observed in the Dgat2 OE group, with fewer sleep bouts and longer bouts, indicating that Dgat2 manipulation alters sleep patterns in these models **(Extended Data Fig. 9, 10a-c).** However, at 7-weeks, sleep behavior in App^{NLG} and *Aβ42* models with *Dgat2 KD* and OE was largely unchanged compared to the

3-week-old flies **(Extended Data Fig. 11a-d).** This suggests that the impact of Dgat2 manipulation on sleep may be age-dependent, with no significant change in older flies.

Dgat2 knockdown suppressed lipid metabolism, restored synaptic loss, and reduced inflammation associated with *App^{NLG} and Aβ42*

We assessed immunostaining in Elav-driven *Dgat2 KD* flies expressing *App^{NLG} and Aβ42* at 3-week to examine potential changes in lipid metabolism and synaptic function. At this early age, we observed that lipid accumulation, typically elevated in *App^{NLG} and Aβ42* models, was significantly reduced in the presence of *Dgat2 KD.* This suggests that *Dgat2 KD* mitigates abnormal lipid buildup associated with AD models. Interestingly, synapsin levels were notably elevated in these flies **(Fig. 6a-c),** indicating improved synaptic function in response to decreased lipid accumulation**.** At 7 weeks, lipid levels remained reduced in the presence of *Dgat2 KD,* suggesting sustained mitigation of lipid dysregulation. However, synapsin levels were unaffected at 7 weeks **(Extended Data Fig. 12a-c),** indicating that neither the expression of App mutant or β-amyloid nor the continued reduction in lipid accumulation due to Dgat2 knockdown, synapsin levels remain unchanged at this age. This suggests that *Dgat2 KD* has a persistent effect on lipid metabolism, but its impact on synaptic function may be age-dependent.

We further examined neuroinflammatory markers. The levels of primary inflammatory cytokines, unpaired1 (Upd1) and, unpaired3 (Upd3), were significantly reduced in *Dgat2 KD* flies, indicating decreased neuroinflammation. However, expression of the JAK/STAT pathway receptors, domeless (Dome) and Hopscotch (Hop) was increased, suggesting that the reduction in inflammation may activate compensatory signaling through this pathway **(Fig. 6d).** We also analyzed the expression of metabolic markers *Abca* and *Dgat2*. In *Dgat2* knockdown flies within both *AppNLG* and *Aβ42* models, *Abca* expression was elevated, suggesting a compensatory response to disrupted lipid metabolism. This upregulation may help maintain lipid homeostasis in neurodegenerative conditions (**Fig. 6e**).

Dgat2 inhibition increased Dgat2 protein and inflammatory gene Ptprq expression in *App^{NLG-F}* mice.

For additional validation, we used mouse brain samples and performed lipid spot staining and GFAP immunofluorescence in the presence of a Dgat2 inhibitor **(Fig. 6f).** In this experiment, we found that lipid spot intensity was significantly increased, contrary to our finding in the flies that the *Dgat2 KD* decreased lipid accumulation **(Fig. 6g).** The contrasting results may arise from species-specific differences in lipid metabolism and compensatory mechanisms, with Drosophila showing reduced lipid accumulation due to direct *Dgat2 KD*, while mice exhibit increased lipid spot intensity possibly as a compensatory response to disrupted lipid homeostasis**.** GFAP level remained unchanged in the presence of Dgat2 inhibitor **(Fig. 6h).** This suggests that Dgat2 inhibition at this dose and frequency does not affect astrocyte activation in $App^{NLG\text{-}F}$ mouse model. In the mouse brain cortical region, Nile Red staining and Adrp expression did not show significant changes **(Extended Data Fig. 12d-i),** indicating that baseline lipid accumulation or storage was unaffected under normal conditions. Nile Red staining revealed an increased trend of number of lipid spots, suggesting enhanced lipid accumulation. This increase in lipid spots was accompanied by an upregulation of Dgat2 level, as indicated by stronger Dgat2 staining, which points to a compensatory mechanism in response to its inhibition. The upregulation of Dgat2 protein likely contributes to the observed increase in lipid droplets, as the brain attempts to maintain lipid homeostasis despite the inhibition of Dgat2.

Consistent with a compensatory upregulation of Dgat2, we observed a significant increase in inflammatory gene Ptprq expression, suggesting a potential upregulation of processes involved in amyloid processing, cell signaling, and lipid transport **(Fig. 6i).** Additionally, the levels of Iba1 protein, a marker of microglial activation, were not unaffected **(Extended Data Fig. 13a, b),** indicating no direct modulation of microglial activation by Dgat2 inhibition. Additionally, other inflammatory markers such as Jak2, Ripk1 and additional AD risk genes, like Bin1, Apoe, Eph, and Ank1 remained unaffected, highlighting a selective modulation of specific inflammatory pathways by Dgat2 inhibition **(Extended Data Fig. 13c-e).**

The expression of potential Dgat2 transcription factors (TFs) was elevated in *App^{NLG} and Aβ42* models and their panneuronal specific KD led to altered sleep circadian activity

To address whether Dgat2 TFs play a role in regulating sleep and circadian activity, we first assessed the relative gene expression levels using qPCR to determine the expression of potential transcriptional regulators of Dgat2. Our results revealed that Eip75b, EcR, Nfat, and Srebp, all of which are involved in lipid metabolism and cellular stress responses, were significantly upregulated in Elav-driven *App^{NLG}, and Elav-Aβ42* model **(Fig. 7a).** Because of their potential in Dgat2 regulation[28-32], these TFs might play a pivotal role in regulating Dgat2 expression and could contribute to the pathophysiology of AD by influencing lipid metabolism, synaptic function, and neuroinflammatory responses. In our next experiment, we examined changes in sleep activity following the KD of specific TFs that regulate Dgat2 expression. Previous results **(Fig. 5 d, e)** shows that *Dgat2 KD* leads to the restoration of sleep activity and reduced sleep fragmentation in the *App^{NLG} and Aβ42* flies' models. Now, with *Dgat2* TF *KD,* we found that total sleep was significantly decreased in both *EcR* and *Srebp KD* flies, indicating that these transcription factors are involved in maintaining overall sleep duration. In contrast, day sleep was notably reduced in *Eip75b KD flies*, as well as in *EcR* and *Srebp* KD flies, indicating that these TFs are involved in regulating daytime sleep. Furthermore, we observed that sleep activity was significantly increased in the KD groups, which supports the overall findings **(Extended Data Fig. 14a)**. We also assessed sleep fragmentation and observed significant changes in this aspect of sleep regulation. Both total and night sleep fragmentation was significantly reduced in the *Nfat KD* group, indicating that Nfat plays a crucial role in maintaining sleep stability and continuity. On the other hand, day sleep TFs may be involved in processes that regulate daytime sleep fragmentation **(Fig.7a, b).** Additionally, *Nfat KD* decreased bout numbers and increased bout length, further supporting the idea that Nfat contributes to the stability of sleep **(Extended Data Fig. 14b, c)**. These findings suggest that different TFs involved in Dgat2 regulation contribute to various aspects of sleep, such as overall duration, timing (day vs. night), and sleep fragmentation **(Fig.7a, b).**

Knock-down of Dgat2 transcription factors (TFs) leads to reduced lipid accumulation and reduced expression of AD linked genes

To further investigate the impact of TF KD on lipid metabolism and synaptic regulation, we assessed lipid and synapsin dysregulation in the Dgat2 TFs KD groups. Our results showed a significant reduction in lipid accumulation in the *Srebp KD, Eip75b KD, and Nfat KD* groups compared to controls **(Fig. 7d, e).** This suggests that these TFs are involved in regulating lipid metabolism and that their KD may help reduce lipid buildup. Interestingly, we also observed that synapsin levels were increased specifically in the *Nfat KD* group, which could indicate a potential compensatory mechanism or a more pronounced effect on synaptic function when *Nfat* is KD **(Fig. 7f).**

Next, we first assessed the role of specific TFs in regulating AD risk genes and found distinct patterns of gene expression changes. Amphiphysin (Amph), Ephrin receptor (Eph), Ankyrin (Ank), Rho GTPase (Rho5), and Neuro-Laz (Nlaz) were specifically upregulated in *Vri KD*, suggesting that *Vri* may regulate these genes, potentially linking them to lipid metabolism and neuroinflammation. Conversely, Abca3, a gene involved in lipid transport, was found to be upregulated in the presence of Eip75b, *EcR*, and *Vri* KD, indicating that these TFs may co-regulate Abca3, expression. Additionally, cas family adaptor protein (P130CAS), a gene linked to cell adhesion and synaptic function, was affected in both Eip75b and *Vri* KD, suggesting that these TFs might also influence pathways regulating neuronal connectivity and function **(Fig. 7g)**.

Inhibition of Dgat2 decreased the expression of Dgat2 transcription factors (TFs) and AD risk genes in the *App^{NLG-F}* mouse model

To further validate these findings, we assessed TF expression in *App^{NLG-F}* mice and found that Nr1h2 (Liver X Receptor alpha, LXRα), a TF involved in lipid regulation, was decreased in the presence of Dgat2 inhibitors, implying that Dgat2 inhibition alters lipid homeostasis at the transcriptional level. However, other TFs such as Srebf1 and Nfat5 remained unchanged, suggesting that Dgat2 inhibition selectively modulates specific lipid-regulating pathways without broadly affecting other TF (**Fig. 7h-i**). Moreover, in the *App^{NLG-F}* mice, the expression of key AD risk genes, Abca7, Rhbdf2, and cass4 was significantly reduced in the presence of Dgat2 inhibitors, suggesting that lipid metabolism modulation through Dgat2 inhibition could potentially downregulate processes involved in

amyloid processing, and lipid transport. These findings suggest a complex relationship between lipid accumulation and synaptic regulation, with different Dgat2 TFs potentially playing distinct roles in lipid homeostasis and synaptic health.

Discussion

AD is characterized by the accumulation of amyloid plaques and tau tangles, leading to cognitive decline and neurodegeneration[54]. Genetic models, such as *Drosophila* expressing APP mutations, offer valuable insights into the mechanisms underlying AD[55]. This study explored the effects of App^{NLG}, as well as the aggregation-prone *Aβ42*) on locomotor function, memory, and lipid metabolism in *Drosophila.* Additionally, we examined the role of Dgat2, a key enzyme in lipid metabolism, through its knockdown and overexpression[56]. To further establish our findings, we used the $App^{NLG\text{-}F}$ mouse model of AD, allowing for cross-species comparison of lipid profiles, neuroinflammation, and gene expression. Through locomotor assays, cognitive test, lipid analysis, and gene expression studies, we aimed to uncover how these genetic modifications influence AD pathogenesis and identify potential therapeutic strategies for mitigating AD-associated dysfunction.

Our findings highlight the complex interplay between amyloid pathology, lipid metabolism, and neuroinflammation across the species using the *Drosophila* and mouse AD models. We observed that male *Drosophila* expressing the *Aβ42* mutation exhibited significant locomotor impairments, particularly reduced climbing ability in the geotaxis assay. Interestingly, the decline was more pronounced in the flies with panneuronal or glial-specific expression of *Aβ42* compared to those expressing the App^{NLG} construct, suggesting that the geotaxis phenotype is mutation-specific **(Fig. 1b).** This aligns with previous studies linking amyloid-related motor deficits to the expression of toxic *Aβ* species[57]. Cognitive assays also revealed a significant memory impairment, particularly in flies expressing *Aβ42* in the mushroom bodies, a key brain region critical for olfactory learning **(Fig. 1c-e)**. This observation underscores the critical role of specific brain regions in cognitive dysfunction in AD, aligning with findings in mammalian models where amyloid pathology in the hippocampus and cortex impairs memory[58].

Our findings demonstrate significant sleep disruptions in *Drosophila* models expressing the *Aβ42* mutation, particularly in terms of sleep fragmentation and altered sleep patterns. These disruptions were more pronounced compared to the APP mutation model, indicating that the *Aβ42* mutation has a stronger impact on sleep quality. The increase in total sleep time, predominantly during the nighttime **(Fig.2a, b),** aligns with previous research showing that AD models often exhibit prolonged sleep durations, especially at night[69, 60]. However, our results also revealed a notable rise in sleep fragmentation, particularly in the Elav- and GLaz-driven models, suggesting that while these flies sleep more, the quality of their sleep is impaired **(Fig.2c, d, f).** This fragmented sleep phenomenon is consistent with clinical observations in AD patients, who often experience fragmented sleep despite longer sleep durations[61, 62]. Furthermore, decreased activity levels, particularly in the Elav-driven model, suggested that the sleep changes are closely tied to disruptions in overall activity and circadian rhythms, as seen in both *Drosophila* and mammalian AD models[61-63]. The persistence of sleep disturbances in older flies suggests that sleep dysregulation is a chronic feature of AD pathology, much like the long-term sleep issues observed in AD patients[65, 66]. The differences in sleep fragmentation patterns between the neuronal and glial-specific models highlight the potential role of glial cells in modulating sleep, with glial-specific expression leading to a distinct pattern of increased daytime sleep bouts and longer bout lengths. This is consistent with recent studies implicating glial activation in the disruption of sleep architecture in AD models[66-68]. Collectively, these results reinforce the idea that sleep disturbances, particularly fragmented sleep, are a central feature of AD pathology and may serve as an early indicator of disease progression.

Evidence from our study provides that lipid dysregulation and synaptic impairment play crucial roles in the progression of AD, with distinct differences in the severity of these alterations between the *Aβ42 and App^{NLG}* models. Lipid accumulation was significantly elevated in both Drosophila and mouse models of AD, particularly in the *Aβ42* model, which exhibited more pronounced lipid deposition compared to the *App^{NLG}* model (**Fig. 3a-d**). This aligns with previous research indicating that dysregulated lipid metabolism, particularly the accumulation of lipid droplets, is a key feature of AD pathogenesis[69]. These lipid imbalances are thought to contribute to cellular stress and dysfunction,

particularly in neurons and glial cells, which may exacerbate the cognitive and behavioral deficits seen in AD[70, 71].

In addition to lipid accumulation, we observed a marked reduction in synapsin expression, a protein crucial for synaptic function **(Fig. 3d).** This finding is consistent with studies showing that synaptic loss and dysfunction are hallmarks of AD, and are often correlated with cognitive decline[72, 73]. The more pronounced reductions in synapsin in the *Aβ42* model suggest that amyloid-β may have a more severe impact on synaptic integrity than other forms of APP mutations[74]. Transitioning to the *App*$^{NLG\text{-}F}$ mouse model further corroborates these findings, showing a significant increase in lipid accumulation and glial activation, particularly with aging, suggesting that lipid dysregulation and neuroinflammation are progressive features of AD pathology **(Fig. 3g-j; Extended Data Fig. 4g-j).** Aging exacerbates lipid accumulation and astrocyte activation, a key aspect of AD progression[75]. Elevated GFAP level, indicative of glial activation, further supports the idea that lipid imbalances are coupled with neuroinflammation in the aging brain[76].

Microglial activation and neuroinflammation play pivotal roles in AD progression, as evidenced by the increased Iba1, a marker for microglial activation, in the *App*$^{NLG\text{-}F}$ mouse model **(Fig. 4a, b).** This age-dependent increase of Iba1 suggests that chronic neuroinflammation becomes more pronounced with advancing age, consistent with studies linking microglial activation to neurodegenerative diseases, including AD[77]**.** The increase in Iba1 is consistent with reports indicating that sustained microglial activation is a driver of neurodegeneration[78, 79.] Furthermore, the observed upregulation of Ptprq **(Fig. 4c)** corroborates the presence of chronic, age-related inflammation in these mice, consistent with other reports on the role of neuroinflammation in AD pathology[80]. Interestingly, the increased expression of key AD risk genes, including Bin1, Rhbdf2, Apoe and Abca7, which are involved in amyloid processing and lipid metabolism **(Fig. 4e),** suggests that amyloid burden or lipid dysmetabolism worsen with age, further implicating lipid pathways in AD progression[81]**.** Furthermore, the elevation of Rhbdf2 and ApoE**,** both of which are linked to neuroinflammation and lipid homeostasis, underscores the role of disrupted lipid pathways in AD risk[82]**.** Collectively, these findings point to a progressive activation of inflammatory and amyloid-related pathways in the *App*$^{NLG\text{-}F}$ model, with aging catalyzing the exacerbation of neuroinflammatory responses. The

combination of these factors highlights the importance of neuroinflammation in driving disease progression in AD and suggests potential therapeutic avenues targeting these pathways.

Our study also explored how Dgat2 expression affects lipid metabolism and neurodegeneration in AD. *Dgat2*, a key enzyme involved in lipid biosynthesis, has been implicated in neuroinflammation and neurodegenerative processes[83, 25]. *Dgat2 KD* and OE in Drosophila models indicate that lipid metabolism plays a critical role in locomotor, cognitive, and sleep deficits associated with AD. *Dgat2 KD* improves locomotor function, specifically in male flies expressing APP-mutant genes *(App^{NLG} and Aβ42),* where KD partially rescues climbing ability **(Fig. 5a).** This suggests that *Dgat2* KD may mitigate some detrimental effects of amyloid-beta aggregation and provide protection against motor impairments seen in AD[84]. Conversely, *Dgat2* OE exacerbates locomotor deficits, supporting the idea that lipid accumulation can worsen AD pathology.

Cognitive function, assessed through the olfactory aversion memory test, mirrored the locomotor results. The *Dgat2 KD* condition rescued memory impairment in both male and female AD models, while *Dgat2* OE had no similar effects **(Fig. 5b, c).** This suggests that *Dgat2* modulation can influence cognitive function, with KD providing a potential protective effect in the context of AD. Interestingly, our sensory acuity test[50] further confirmed these trends, reinforcing the notion that *Dgat2* manipulation, particularly KD, can help preserve cognitive function in AD models. In terms of sleep, both *Dgat2* KD and OE conditions led to increased total sleep and reduced sleep fragmentation at 3 weeks of age **(Fig. 5d, e).** These results indicate that *Dgat2* manipulation does not drastically alter sleep behavior in younger flies, but that the effects on sleep are age dependent[85]. However, in older AD flies (7 weeks), sleep patterns were largely unchanged by Dgat2 modulation, suggesting that the effects of lipid metabolism manipulation on sleep are less pronounced with age **(Extended Data Fig. 9, 10a-c, 11a-d).** These findings highlight the complexity of lipid metabolism's role in neurodegenerative diseases, with age and disease progression influencing the extent of *Dgat*2's impact on sleep, cognition, and motor function.

We explored the effect of *Dgat2 KD* on lipid metabolism and neuroinflammation in Drosophila and mouse models of AD. *Dgat2* KD significantly reduces lipid accumulation,

a hallmark of AD pathology, and increases synapsin levels **(Fig. 6a-c).** This improvement in synapsin level supports the idea that reducing lipid accumulation may help the preservation of synaptic integrity, a crucial aspect of cognitive function in AD models[86]**.** We also observed reduced expression of Upd1 and Upd3 cytokines associated with neuroinflammation in AD **(Extended Data Fig.8)**. Interestingly, the expression of Dome and Hop receptors, which are integral to the JAK/STAT signaling pathway, remained unaffected, suggesting that *Dgat2 KD* effect on inflammation is mediated through lipid-related mechanisms**,** not directly via the JAK/STAT pathway[87]**.** Further validation in the APP mouse model using a Dgat2 inhibitor revealed an increase in lipid spots, consistent with a compensatory upregulation of *Dgat2* **(Fig. 6f, g).** GFAP expression, a marker of astrocyte activation, remained unchanged (Fig. 6h), indicating that Dgat2 inhibition, despite increased lipid spot intensity, does not directly impact astrocyte-mediated neuroinflammation. Similarly, microglial activation, assessed through Iba1 levels, was unaffected by Dgat2 inhibition (Extended Data Fig. 13a, b). These findings contrast with prior reports suggesting lipid metabolism alterations modulate both astrocytic and microglial responses in AD. However, we observed a significant increase in Ptprq expression and a decrease in key AD risk genes like Abca7, Cass4, and Rhbdf2 (**Fig. 6i**), suggesting Dgat2 modulation selectively impacts specific lipid dysregulation and neuroinflammation pathways in AD[88, 89].

Finally, we explore the regulatory mechanisms underlying lipid dysregulation, neuroinflammation, and sleep dysfunctions in AD models. Key TFs such as Eip75b, Nfat, and Srebp were upregulated in Elav-driven AD models **(Fig. 7a) These TFs** regulate lipid metabolism and cellular stress responses, contributing to AD pathophysiology by affecting lipid homeostasis, synaptic function, and neuroinflammation[90]. Further investigation into the role of the impact of specific TF KDs in sleep activity revealed significant alternations in the sleep patterns, with *EcR and Srebp KD* flies exhibiting decreased total sleep, and altered sleep continuity **(Fig. 7b).** These findings underscore the complex relationship between lipid metabolisms and sleep regulation in AD models[90, 47].

In conclusion, both panneuronal and glial-specific expression of *App*^{NLG} *and Aβ42* led to severe impairments in locomotor and cognitive functions, enhanced lipid accumulation, and decreased synapsin levels. *Dgat2 KD* partially rescued these detrimental effects, providing insight into the potential therapeutic role of Dgat2 in *Drosophila.* Further research into the molecular markers involved in these processes and the role of Dgat2 modulation could provide valuable targets for mitigating neurodegeneration in *App*$^{NLG-F}$ mouse model (**Fig. 8**).

Funding: This work was partially supported by National Institutes of Health (NIH) grants AG065992 and RF1NS133378 to G.C.M. P30 AG050886 (GM and JZ), T32 HL007457 (JK), R01AG072895 (JZ), R01ES034846 (JZ), R21AG081687 (JZ). This work is also supported by UAB Startup funds 3123226 and 3123227 to G.C.M.

Author Contribution: GCM, JZ, JK, XO, and AY designed the experiments including feedback from JJ. AY performed most sleep and all geotaxis experiments. AY performed the analysis of sleep parameters, qPCR experiments, and analysis of both *Drosophila* and mouse samples. OX performed all immunofluorescence staining of mouse brain samples. MB performed most memory assays. JCW processes all brain samples of the *Drosophila* brain and performs immunofluorescence staining and analyses with help from GCM. KM collected some sleep activity and memory data and performed immunoblot analyses. JC has performed Dgat2 inhibitor dosing in mice. AY performed analysis and analyzed all the data including statistical analyses with help from GCM and JZ. AY prepared the paper with GCM's input. All the authors reviewed the manuscript and provided their feedback.

Acknowledgment: Stocks obtained from the Bloomington Drosophila Stock Center were used in this study.

Competing interests: The authors declare no competing interests.

Additional Information: Extended data is available for this paper at available in a separate PDF file

Data source file: Source data is available for this paper at source data in a single Excel sheet.

Online Data Sharing: NA

References

1. Western, Daniel, et al. Proteogenomic analysis of human cerebrospinal fluid identifies neurologically relevant regulation and implicates causal proteins for Alzheimer's disease. *Nature Genetics* (2024): 1-13.
2. Nichols, Emma, et al. Estimation of the global prevalence of dementia in 2019 and forecasted prevalence in 2050: an analysis for the Global Burden of Disease Study 2019. *The Lancet Public Health* 7.2 (2022): e105-e125.
3. Bartoletti-Stella, Anna, et al. Identification of rare genetic variants in Italian patients with dementia by targeted gene sequencing. *Neurobiology of Aging* 66 (2018): 180-e23.
4. Uddin, Md Sahab, et al. Revisiting the role of brain and peripheral Aβ in the pathogenesis of Alzheimer's disease. *Journal of the Neurological Sciences* 416 (2020): 116974.
5. Nikom, David, and Sika Zheng. Alternative splicing in neurodegenerative disease and the promise of RNA therapies. *Nature Reviews Neuroscience* 24.8 (2023): 457-473.
6. Leng, Fangda, and Paul Edison. Neuroinflammation and microglial activation in Alzheimer disease: where do we go from here?. *Nature Reviews Neurology* 17.3 (2021): 157-172.
7. Daynes, Raymond A., and Dallas C. Jones. Emerging roles of PPARs in inflammation and immunity. *Nature Reviews Immunology* 2.10 (2002): 748-759.
8. Munkácsy, Erin, et al. Neuronal-specific proteasome augmentation via Prosβ5 overexpression extends lifespan and reduces age-related cognitive decline. Aging cell 18.5 (2019): e13005.
9. Ralhan, Isha, et al. Lipid droplets in the nervous system. *Journal of Cell Biology* 220.7 (2021): e202102136.
10. Martens, Yuka A., et al. ApoE Cascade Hypothesis in the pathogenesis of Alzheimer's disease and related dementias. *Neuron* 110.8 (2022): 1304-1317.
11. Picard, Cynthia, et al. Alterations in cholesterol metabolism–related genes in sporadic Alzheimer's disease. *Neurobiology of aging* 66 (2018): 180-e1.

12. Chen, Feng, et al. The vascular contribution of apolipoprotein E to Alzheimer's disease. *Brain* (2024): awae156.
13. Singh, Rajat, and Ana Maria Cuervo. Lipophagy: connecting autophagy and lipid metabolism. *International journal of cell biology* 2012.1 (2012): 282041.
14. Ates, Gamze, et al. CMS121, a fatty acid synthase inhibitor, protects against excess lipid peroxidation and inflammation and alleviates cognitive loss in a transgenic mouse model of Alzheimer's disease. *Redox Biology* 36 (2020): 101648.
15. Daugherty, Daniel, et al. A novel Alzheimer's disease drug candidate targeting inflammation and fatty acid metabolism. *Alzheimer's Research & Therapy* 9 (2017): 1-17.
16. Eraso-Pichot, Abel, et al. GSEA of mouse and human mitochondriomes reveals fatty acid oxidation in astrocytes. *Glia* 66.8 (2018): 1724-1735.
17. Edmond, J., et al. Capacity for substrate utilization in oxidative metabolism by neurons, astrocytes, and oligodendrocytes from developing brain in primary culture. *Journal of neuroscience research* 18.4 (1987): 551-561.
18. Namgaladze, Dmitry, and Bernhard Brüne. Macrophage fatty acid oxidation and its roles in macrophage polarization and fatty acid-induced inflammation. *Biochimica et Biophysica Acta (BBA)-Molecular and Cell Biology of Lipids* 1861.11 (2016): 1796-1807.
19. Song, Gyun Jee, and Kyoungho Suk. Pharmacological modulation of functional phenotypes of microglia in neurodegenerative diseases. *Frontiers in aging neuroscience* 9 (2017): 139.
20. Liu, Bingrun, et al. Isovitexin-mediated regulation of microglial polarization in lipopolysaccharide-induced neuroinflammation via activation of the CaMKKβ/AMPK-PGC-1α signaling axis. *Frontiers in immunology* 10 (2019): 2650.
21. Shie, Feng-Shiun, et al. Diet-induced hypercholesterolemia enhances brain Aβ accumulation in transgenic mice. Neuroreport 13.4 (2002): 455-459.
22. Refolo, Lorenzo M., et al. Hypercholesterolemia accelerates the Alzheimer's amyloid pathology in a transgenic mouse model. *Neurobiology of disease* 7.4 (2000): 321-331.

23. Huang, Helen Xuexia, et al. Mass spectrometry imaging highlights dynamic patterns of lipid co-expression with Aβ plaques in mouse and human brains. *Journal of Neurochemistry* (2024).
24. Adamovich, Yaarit, et al. Circadian clocks and feeding time regulate the oscillations and levels of hepatic triglycerides. *Cell metabolism* 19.2 (2014): 319-330.
25. Moraes, Ruan CM, et al. Apolipoprotein E Induces Lipid Accumulation Through Dgat2 That Is Prevented with Time-Restricted Feeding in Drosophila. *Genes* 15.11 (2024): 1376.
26. Livelo, Christopher, et al. Time-restricted feeding mediated modulation of microbiota leads to changes in muscle physiology in Drosophila obesity models. *Aging Cell* (2024): e14382.
27. Livelo, Christopher, et al. Time-restricted feeding promotes muscle function through purine cycle and AMPK signaling in Drosophila obesity models. *Nature communications* 14.1 (2023): 949.
28. Hoedjes, Katja M., et al. A single nucleotide variant in the PPARγ-homolog Eip75B affects fecundity in Drosophila. Molecular biology and evolution 40.2 (2023): msad018.
29. Uyehara, Christopher M., and Daniel J. McKay. Direct and widespread role for the nuclear receptor EcR in mediating the response to ecdysone in Drosophila. Proceedings of the National Academy of Sciences 116.20 (2019): 9893-9902.
30. Yang, Teddy TC, et al. Role of transcription factor NFAT in glucose and insulin homeostasis. Molecular and cellular biology 26.20 (2006): 7372-7387.
31. Rong, Shunxing, et al. DGAT2 inhibition blocks SREBP-1 cleavage and improves hepatic steatosis by increasing phosphatidylethanolamine in the ER. Cell metabolism 36.3 (2024): 617-629.
32. Yenilmez, Batuhan, et al. An RNAi therapeutic targeting hepatic DGAT2 in a genetically obese mouse model of nonalcoholic steatohepatitis. Molecular Therapy 30.3 (2022): 1329-1342.

33. Rong, Shunxing, et al. DGAT2 inhibition blocks SREBP-1 cleavage and improves hepatic steatosis by increasing phosphatidylethanolamine in the ER. Cell metabolism 36.3 (2024): 617-629.
34. Prakash, Priya, et al. Amyloid β induces lipid droplet-mediated microglial dysfunction in Alzheimer's disease. *bioRxiv* (2023).
35. Panda, Satchidananda, John B. Hogenesch, and Steve A. Kay. Circadian rhythms from flies to human. *Nature* 417.6886 (2002): 329-335.
36. Hardin, Paul E., and Satchidananda Panda. Circadian timekeeping and output mechanisms in animals. *Current opinion in neurobiology* 23.5 (2013): 724-731.
37. Austad, Steven N., et al. Targeting whole body metabolism and mitochondrial bioenergetics in the drug development for Alzheimer's disease. *Acta Pharmaceutica Sinica B* 12.2 (2022): 511-531.
38. Villanueva, Jesús E., et al. Time-restricted feeding restores muscle function in Drosophila models of obesity and circadian-rhythm disruption. *Nature communications* 10.1 (2019): 2700.
39. Yokoyama, Miyabishara, et al. Mouse models of Alzheimer's disease. Frontiers in Molecular Neuroscience 15 (2022): 912995.
40. Melkani, Girish C., et al. Huntington's disease-induced cardiac amyloidosis is reversed by modulating protein folding and oxidative stress pathways in the Drosophila heart. *PLoS Genetics* 9.12 (2013): e1004024.
41. Gill, Shubhroz, et al. Time-restricted feeding attenuates age-related cardiac decline in Drosophila. *Science* 347.6227 (2015): 1265-1269.
42. Villanueva, Jesús E., et al. Time-restricted feeding restores muscle function in Drosophila models of obesity and circadian-rhythm disruption. *Nature Communications* 10.1 (2019): 2700.
43. Koushika, Sandhya P., Michael J. Lisbin, and Kalpana White. ELAV, a Drosophila neuron-specific protein, mediates the generation of an alternatively spliced neural protein isoform. Current Biology 6.12 (1996): 1634-1641.
44. Sanchez, Diego, et al. Loss of glial lazarillo, a homolog of apolipoprotein D, reduces lifespan and stress resistance in Drosophila. Current Biology 16.7 (2006): 680-686.

45. Aso, Yoshinori, et al. The mushroom body of adult Drosophila characterized by GAL4 drivers. Journal of neurogenetics 23.1-2 (2009): 156-172.
46. Guo, Yiming, et al. Diurnal expression of Dgat2 induced by time-restricted feeding maintains cardiac health in the Drosophila model of circadian disruption. *Aging Cell* (2024): e14169.
47. Osterwalder, Thomas, et al. A conditional tissue-specific transgene expression system using inducible GAL4. Proceedings of the National Academy of Sciences 98.22 (2001): 12596-12601.
48. Thrupp, Nicola, Bart De Strooper, and Mark Fiers. Transcriptomics to study the cellular phase of Alzheimer's Disease. (2023).
49. Chocron, E. Sandra, et al. Genetic and pharmacologic proteasome augmentation ameliorates Alzheimer’s-like pathology in mouse and fly APP overexpression models. Science advances 8.23 (2022): eabk2252.
50. Meschi, Eleonora, et al. Compensatory enhancement of input maintains aversive dopaminergic reinforcement in hungry Drosophila. Neuron (2024).
51. Abou Daya, Farah, et al. Identifying novel links between cardiovascular disease and insomnia by Drosophila modeling of genes from a pleiotropic GWAS locus. *bioRxiv* (2023): 2023-07.
52. Watson, John, Jonathan R. Roth, and Girish C. Melkani. Direct Cryosectioning of Drosophila Heads for Enhanced Brain Fluorescence Staining and Immunostaining. *Journal of Visualized Experiments (JoVE)* 216 (2025): e67791.
53. Roth, Jonathan R., et al. Rapamycin reduces neuronal mutant huntingtin aggregation and ameliorates locomotor performance in Drosophila. Frontiers in Aging Neuroscience 15 (2023): 1223911.
54. Zhang, Huiqin, et al. Interaction between Aβ and tau in the pathogenesis of Alzheimer's disease. *International journal of biological sciences* 17.9 (2021): 2181.
55. Padmanabhan, Pranesh, and Jürgen Götz. Clinical relevance of animal models in aging-related dementia research. *Nature Aging* 3.5 (2023): 481-493.
56. Rong, Shunxing, et al. DGAT2 inhibition blocks SREBP-1 cleavage and improves hepatic steatosis by increasing phosphatidylethanolamine in the ER. *Cell metabolism* 36.3 (2024): 617-629.

57. Sun, Zhen-Dong, et al. Toxicities of amyloid-beta and tau protein are reciprocally enhanced in the Drosophila model. *Neural regeneration research* 17.10 (2022): 2286-2292.
58. Polis, Baruh, and Abraham O. Samson. Addressing the Discrepancies Between Animal Models and Human Alzheimer's Disease Pathology: Implications for Translational Research. *Journal of Alzheimer's Disease* Preprint (2024): 1-20.
59. Meyer, Nicholas, et al. Circadian rhythms and disorders of the timing of sleep. *The Lancet* 400.10357 (2022): 1061-1078.
60. Insel, Philip S., et al. Association of sleep and β-amyloid pathology among older cognitively unimpaired adults. *JAMA Network Open* 4.7 (2021): e2117573-e2117573.
61. Duncan, M. J., et al. Chronic fragmentation of the daily sleep-wake rhythm increases amyloid-beta levels and neuroinflammation in the 3xTg-AD mouse model of Alzheimer's disease. *Neuroscience* 481 (2022): 111-122.
62. Winer, Joseph R., et al. Association of short and long sleep duration with amyloid-β burden and cognition in aging. *JAMA neurology* 78.10 (2021): 1187-1196.
63. Majcin Dorcikova, Michaëla, et al. Circadian clock disruption promotes the degeneration of dopaminergic neurons in male Drosophila. *Nature Communications* 14.1 (2023): 5908.
64. Peter-Derex, Laure, et al. Sleep and Alzheimer's disease. *Sleep medicine reviews* 19 (2015): 29-38.
65. Minakawa, Eiko N., et al. Chronic sleep fragmentation exacerbates amyloid β deposition in Alzheimer's disease model mice. *Neuroscience letters* 653 (2017): 362-369.
66. Bellesi, Michele, et al. Sleep loss promotes astrocytic phagocytosis and microglial activation in mouse cerebral cortex. *Journal of Neuroscience* 37.21 (2017): 5263-5273.
67. Garofalo, Stefano, et al. Role of glia in the regulation of sleep in health and disease. *Compr. Physiol* 10.2 (2020): 687-712.

68. Gentry, Nicholas W., et al. Microglia are involved in the protection of memories formed during sleep deprivation. *Neurobiology of Sleep and Circadian Rhythms* 12 (2022): 100073.
69. Liu, Yue, et al. Plasma lipidome is dysregulated in Alzheimer's disease and is associated with disease risk genes. *Translational psychiatry* 11.1 (2021): 344.
70. Fan, Yong-Gang, et al. Vitamin D deficiency exacerbates Alzheimer-like pathologies by reducing antioxidant capacity. *Free Radical Biology and Medicine* 161 (2020): 139-149.
71. Keeney, Jeriel TR, et al. Dietary vitamin D deficiency in rats from middle to old age leads to elevated tyrosine nitration and proteomics changes in levels of key proteins in brain: implications for low vitamin D-dependent age-related cognitive decline. *Free Radical Biology and Medicine* 65 (2013): 324-334.
72. Lan, Guoyu, et al. Association of presynaptic loss with Alzheimer's disease and cognitive decline. *Annals of Neurology* 92.6 (2022): 1001-1015.
73. Saroja, Sivaprakasam R., et al. Differential expression of tau species and the association with cognitive decline and synaptic loss in Alzheimer's disease. *Alzheimer's & Dementia* 18.9 (2022): 1602-1615.
74. Piccoli, Tommaso, et al. Biomarkers related to synaptic dysfunction to discriminate alzheimer's disease from other neurological disorders. *International Journal of Molecular Sciences* 23.18 (2022): 10831.
75. Emre, Ceren, et al. Age-related changes in brain phospholipids and bioactive lipids in the APP knock-in mouse model of Alzheimer's disease. *Acta neuropathologica communications* 9.1 (2021): 116.]
76. Schuitemaker, Alie, et al. Microglial activation in healthy aging. *Neurobiology of aging* 33.6 (2012): 1067-1072.
77. Kinney, Jefferson W., et al. Inflammation as a central mechanism in Alzheimer's disease. *Alzheimer's & Dementia: Translational Research & Clinical Interventions* 4 (2018): 575-590.
78. Agrawal, Ishan, and Sushmita Jha. Mitochondrial dysfunction and Alzheimer's disease: Role of microglia. *Frontiers in aging neuroscience* 12 (2020): 559682.

79. Sakuraba, Juichi, et al. Substrate specificity of R3 receptor-like protein-tyrosine phosphatase subfamily toward receptor protein-tyrosine kinases. *Journal of Biological Chemistry* 288.32 (2013): 23421-23431.
80. Prendecki, Michał, et al. Genetic factors related to the immune system in subjects at risk of developing Alzheimer's disease. *Journal of Integrative Neuroscience* 19.2 (2020): 359-371.
81. De Jager, Philip L., et al. Alzheimer's disease: early alterations in brain DNA methylation at ANK1, BIN1, RHBDF2 and other loci. *Nature neuroscience* 17.9 (2014): 1156-1163.
82. Stone, Scot J., et al. The endoplasmic reticulum enzyme DGAT2 is found in mitochondria-associated membranes and has a mitochondrial targeting signal that promotes its association with mitochondria. *Journal of Biological Chemistry* 284.8 (2009): 5352-5361.
83. Kang, Jihong, and Serge Rivest. Lipid metabolism and neuroinflammation in Alzheimer's disease: a role for liver X receptors. *Endocrine reviews* 33.5 (2012): 715-746.
84. Broussard, Josiane, and Matthew J. Brady. The impact of sleep disturbances on adipocyte function and lipid metabolism. *Best Practice & Research Clinical Endocrinology & Metabolism* 24.5 (2010): 763-773.
85. Kao, Yu-Chia, et al. Lipids and Alzheimer’s disease. *International journal of molecular sciences* 21.4 (2020): 1505.
86. Jain, Mayank, et al. Role of JAK/STAT in the neuroinflammation and its association with neurological disorders. *Annals of neurosciences* 28.3-4 (2021): 191-200.
87. Iglesias, José, Ludis Morales, and George E. Barreto. Metabolic and inflammatory adaptation of reactive astrocytes: role of PPARs. *Molecular neurobiology* 54 (2017): 2518-2538.
88. Marschallinger, Julia, et al. Lipid-droplet-accumulating microglia represent a dysfunctional and proinflammatory state in the aging brain. *Nature neuroscience* 23.2 (2020): 194-208.

89. Ang, Mary Jasmin, and Changjong Moon. SREBP and central nervous system disorders: genetic overlaps revealed by in silico analysis. *Journal of Integrative Neuroscience* 21.3 (2022): 95.
90. Li, Yongjun, et al. Ecdysone acts through cortex glia to regulate sleep in Drosophila. *Elife* 12 (2023): e81723.
91. Deota, Shaunak, et al. Diurnal transcriptome landscape of a multi-tissue response to time-restricted feeding in mammals. *Cell metabolism* 35.1 (2023): 150-165.

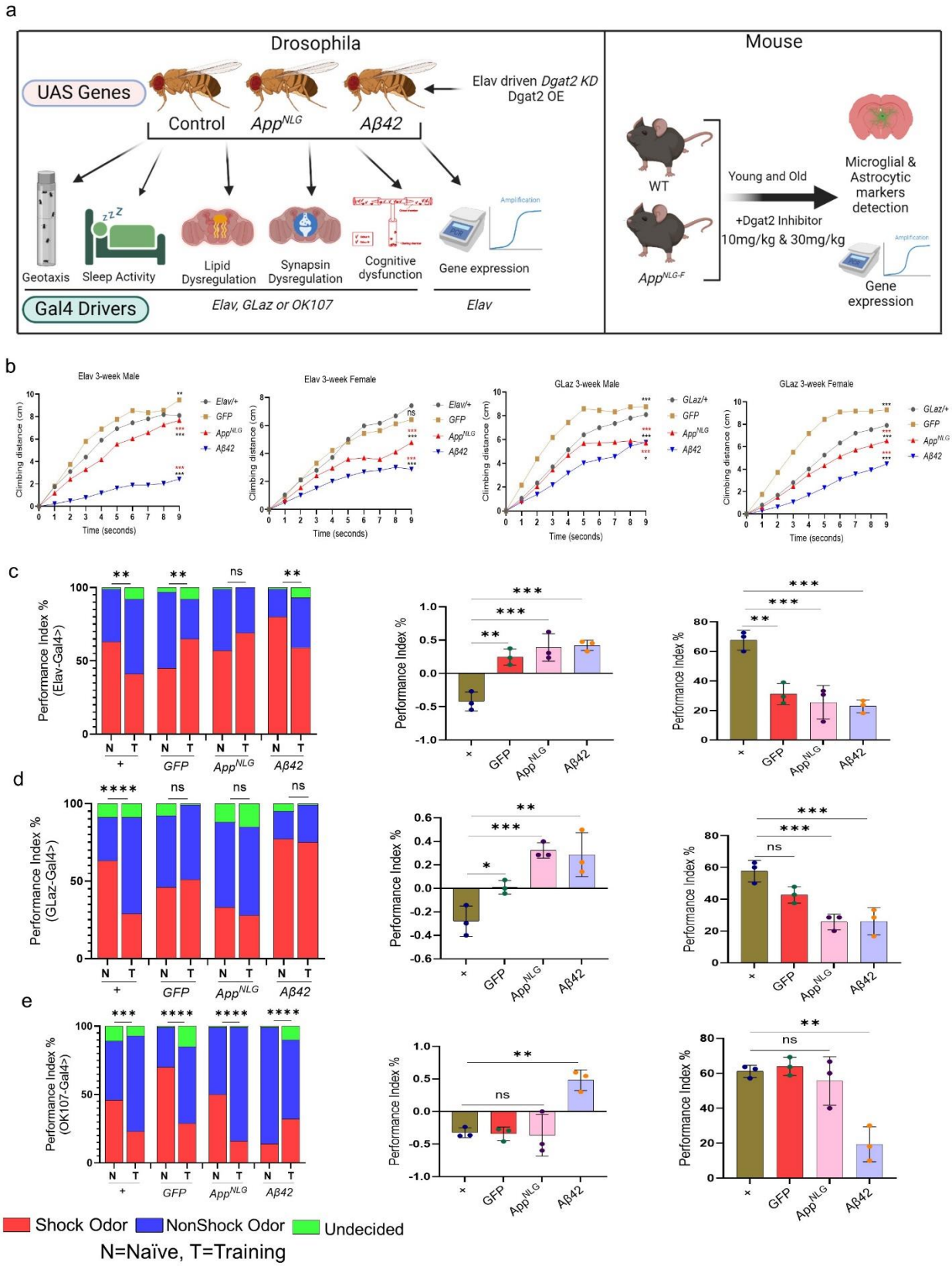
a
Drosophila
Mouse
UAS Genes
Control
App^NLG
Aβ42
Elav driven Dgat2 KD
Dgat2 OE
Geotaxis
Sleep Activity
Lipid Dysregulation
Synapsin Dysregulation
Cognitive dysfunction
Gene expression
Gal4 Drivers
Elav, GLaz or OK107
Elav
WT
App^NLG-F
Young and Old
+Dgat2 Inhibitor
10mg/kg & 30mg/kg
Microglial & Astrocytic markers detection
Gene expression
b
Elav 3-week Male
Elav 3-week Female
GLaz 3-week Male
GLaz 3-week Female
Climbing distance (cm)
Time (seconds)
Elav/+
GLaz/+
GFP
App^NLG
Aβ42
c
Performance Index % (Elav-Gal4>)
Performance Index %
N T
+
GFP
App^NLG
Aβ42
d
Performance Index % (GLaz-Gal4>)
e
Performance Index % (OK107-Gal4>)
Shock Odor
NonShock Odor
Undecided
N=Naïve, T=Training

Fig.1| Panneuronal and glial-specific expression of *App^{NLG} and Aβ42* led to compromised locomotor and cognitive performance. a, Flow chart depicting the experimental setup. Each UAS gene was crossed with the region-specific Gal-4 drivers. To explore the contribution of Dgat2 in *Aβ42 and App* accumulation, we performed Elav-driven *Dgat2 KD* and Dgat2 OE in *Drosophila* and used an *App^{NLG-F}* mouse model with Dgat2 inhibitor**. b,** Negative geotaxis assay of Elav and GLaz drove A*pp^{NLG} and Aβ42* models in 3-week males and females (red asterisk denotes significance with GFP while black asterisks, ns, denotes significance with Elav/+ and/ or GLaz/+). **c-e (Left panels only),** *App^{NLG,} and Aβ42* models show deficits in olfactory aversion training in 3-week-old male flies in Elav **c,** GLaz **d,** and OK107 **e,** driven models; data combined from triplicate assays. Significance was based on the chi-square test. Values are shown as the percentage of flies in each chamber at the end of the assay. **c-e (middle panels only),** the difference between fly decisions, in 3-week-old male flies in Elav **c,** GLaz **d,** and OK107 **e. c-e, (right panels only),** flies avoiding shock odor in Elav **c,** GLaz **d,** and OK107 **e,** driven *App^{NLG} and Aβ42* models. Data = mean ± SD. One-way ANOVA with Tukey's multiple comparisons test was performed (**Left and right panels only**). Mixed LM (Linear model) Effects comparisons were performed for geotaxis, n=3 replicates per group and each group had 10 flies. *p<0.05, **p<0.01 and ***p<0.001, n.s = not significant (an asterisk denotes significance for the average of all three replicates). Raw data and *p values* are provided in the source data.

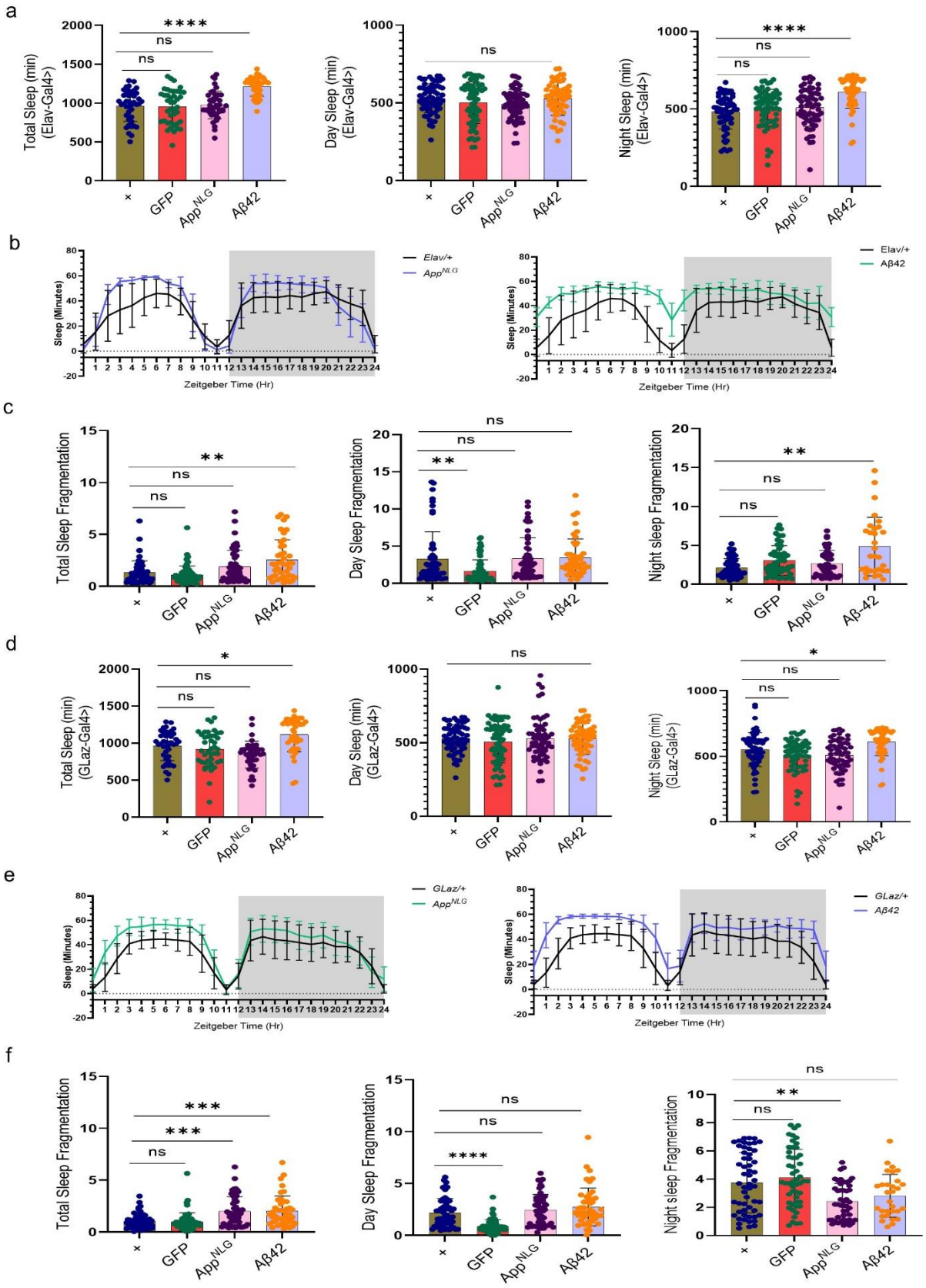
a
Total Sleep (min) (Elav-Gal4>)
Day Sleep (min) (Elav-Gal4>)
Night Sleep (min) (Elav-Gal4>)
****
ns
GFP
App NLG
Aβ42
b
Sleep (Minutes)
Zeitgeber Time (Hr)
Elav/+
App NLG
Aβ42
c
Total Sleep Fragmentation
Day Sleep Fragmentation
Night sleep Fragmentation
**
d
Total Sleep (min) (GLaz-Gal4>)
Day Sleep (min) (GLaz-Gal4>)
Night Sleep (min) (GLaz-Gal4>)
*
e
GLaz/+
App NLG
Aβ42
f
***
****

Fig. 2 | Panneuronal and glial-specific expression of A*β42* has compromised circadian activity and sleep quality compared to *App*^{NLG} which worsens with age

a, Total, day and night sleep (in minutes) in Elav-driven *App*^{NLG} and A*β42 m*odels. **b,** Sleep profiles at different zeitgeber time (hr.) in Elav-driven *App*^{NLG} and A*β42* models only compared to their respective controls. **c,** Total, day and night sleep fragmentation in Elav-driven *App*^{NLG} and A*β42* models. **d,** Total, day and night sleep in (in minutes) in GLaz-driven *App*^{NLG} and A*β42* models. **e,** Sleep profiles at different zeitgeber time (hr.) in GLaz-driven *App*^{NLG} and A*β42* models only compared to their respective controls. **f,** Total, day and night sleep fragmentation in GLaz-driven *App*^{NLG} and A*β42* models. All experiments were performed in 3-week-old males only. Data = mean ± SD. Non-parametric One-way ANOVA with multiple comparisons done with the Kruskal Wallis test was performed for sleep activity and sleep fragmentation. Each dot represents number of flies. *$p < 0.05$; **$p < 0.01$; *** $p < 0.001$; ns = not significant (an asterisk denotes significance for the average of all three replicates). Raw data and *p values* are provided in the source data.

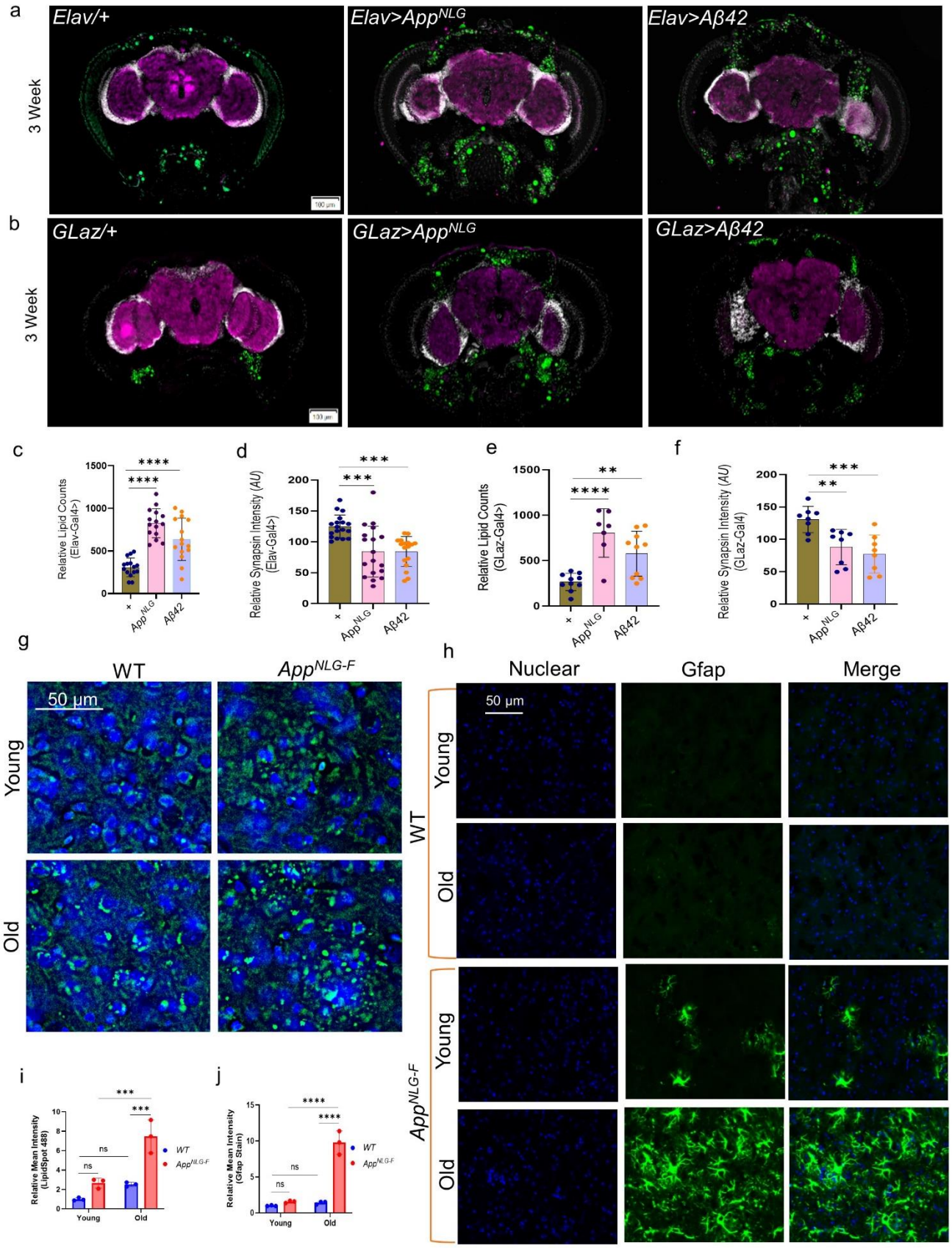
a
Elav/+
Elav>App^NLG
Elav>Aβ42
3 Week
b
GLaz/+
GLaz>App^NLG
GLaz>Aβ42
3 Week
c
Relative Lipid Counts (Elav-Gal4>)
d
Relative Synapsin Intensity (AU) (Elav-Gal4>)
e
Relative Lipid Counts (GLaz-Gal4>)
f
Relative Synapsin Intensity (AU) (GLaz-Gal4)
+
App^NLG
Aβ42
g
WT
App^NLG-F
50 μm
Young
Old
h
Nuclear
Gfap
Merge
50 μm
WT
Young
Old
App^NLG-F
Young
Old
i
Relative Mean Intensity (LipidSpot 488)
ns
WT
App^NLG-F
Young
Old
j
Relative Mean Intensity (Gfap Stain)
ns
WT
App^NLG-F
Young
Old

Fig. 3 | *App^{NLG} and Aβ42* induce lipid accumulation and synapsin reduction in Drosophila, while *App^{NLG-F}* mice show cortical lipid build-up and astrocyte activation. a-b, Representative image showing the expression of lipid accumulation (green, Lipid spot); synaptic loss (purple, anti SYNORF1), a marker of neurodegeneration; and DAPI (white), in the brains of Elav and GLaz-driven *App^{NLG} and Aβ42* flies**. c-f,** Quantification of the expression level of relative lipid counts **c, e,** and synapsin intensity **d, f,** in Elav and GLaz-driven *App^{NLG} and Aβ42* flies. All experiments were performed in 3-week-old flies. **g,** Representative images showing lipid spot intensity (green), indicating lipid accumulation; and DAPI (blue), in the mouse brains of young and old wild type (WT) and *App^{NLG-F}* models. **h,** Representative images showing the immunostaining of Gfap, a marker of astrocyte activation; and DAPI (blue), in the mouse brains of young and old wild type (WT) and *App^{NLG-F}* models**. i-j,** Quantification of the intensity of lipid spots and relative mean intensity of Gfap immunostaining. Fold changes of fluorescence intensity were calculated relative to controls. Data = mean ± SD. One-way ANOVA with Tukey's multiple comparisons test was performed for flies' data, with 5-6 flies per group. Two-way ANOVA with multiple comparisons done with Uncorrected Fisher's LSD test was performed for mouse data, with n=3 mice per group. *$p < 0.05$; **p < 0.01; ***$p < 0.001$; ns = not significant (an asterisk denotes significance for the average of all three replicates). Raw data and *p values* are provided in the source data.

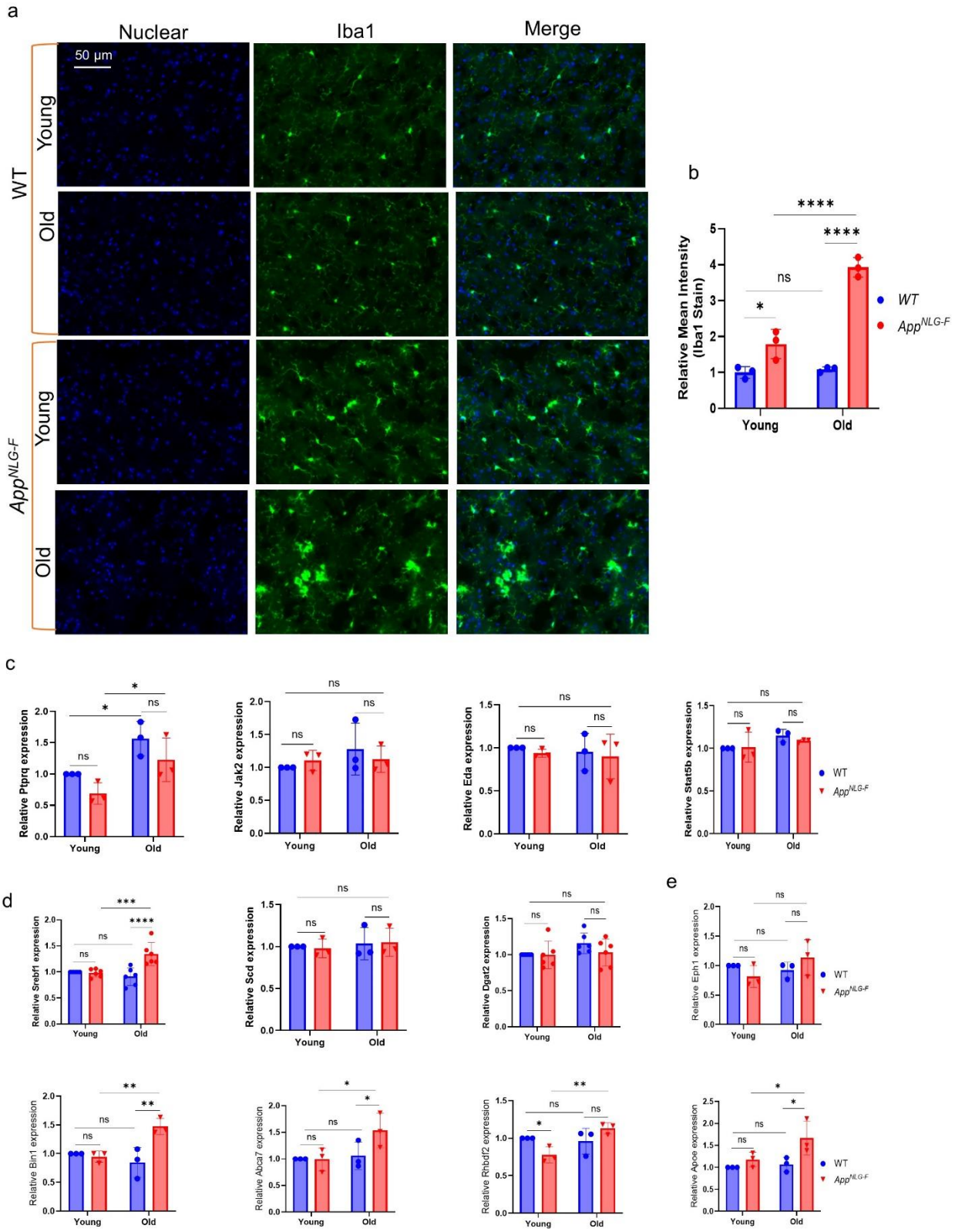
a
Nuclear
Iba1
Merge
50 μm
WT
Young
Old
App^NLG-F
Young
Old
b
Relative Mean Intensity (Iba1 Stain)
Young
Old
WT
App^NLG-F
c
Relative Ptprq expression
Relative Jak2 expression
Relative Eda expression
Relative Stat5b expression
d
Relative Srebf1 expression
Relative Scd expression
Relative Dgat2 expression
e
Relative Eph1 expression
Relative Bin1 expression
Relative Abca7 expression
Relative Rhbdf2 expression
Relative Apoe expression

Fig. 4 | Age-dependent increase in neuroinflammation and AD risk gene expression in a mouse model of *App*$^{NLG-F}$. a, Immunofluorescence staining of Iba1 protein in microglia within the cortex region of the brain of WT and *App*$^{NLG-F}$ mice at young and old age. **b,** Quantification of the Iba1 immunostaining intensity in **a**; n=3 mice per group. **c-e,** Quantitative PCR quantification of the relative expression level of inflammatory genes, Ptprq, Jak2, Eda, and Stat5b **c,** metabolic genes, srebf1, scd and Dgat2 **d,** and AD risk genes, Bin1, Abca7, Rhbdf2 and Apoe **e,** in young and old WT and *App*$^{NLG-F}$ mice. Data = mean ± SD. Two-way ANOVA with multiple comparisons done with Uncorrected Fisher's LSD test was performed. *$p < 0.05$; **$p < 0.01$; ***$p < 0.001$; ns = not significant (an asterisk denotes significance for the average of all three replicates). Raw data and *p values* are provided in the source data.

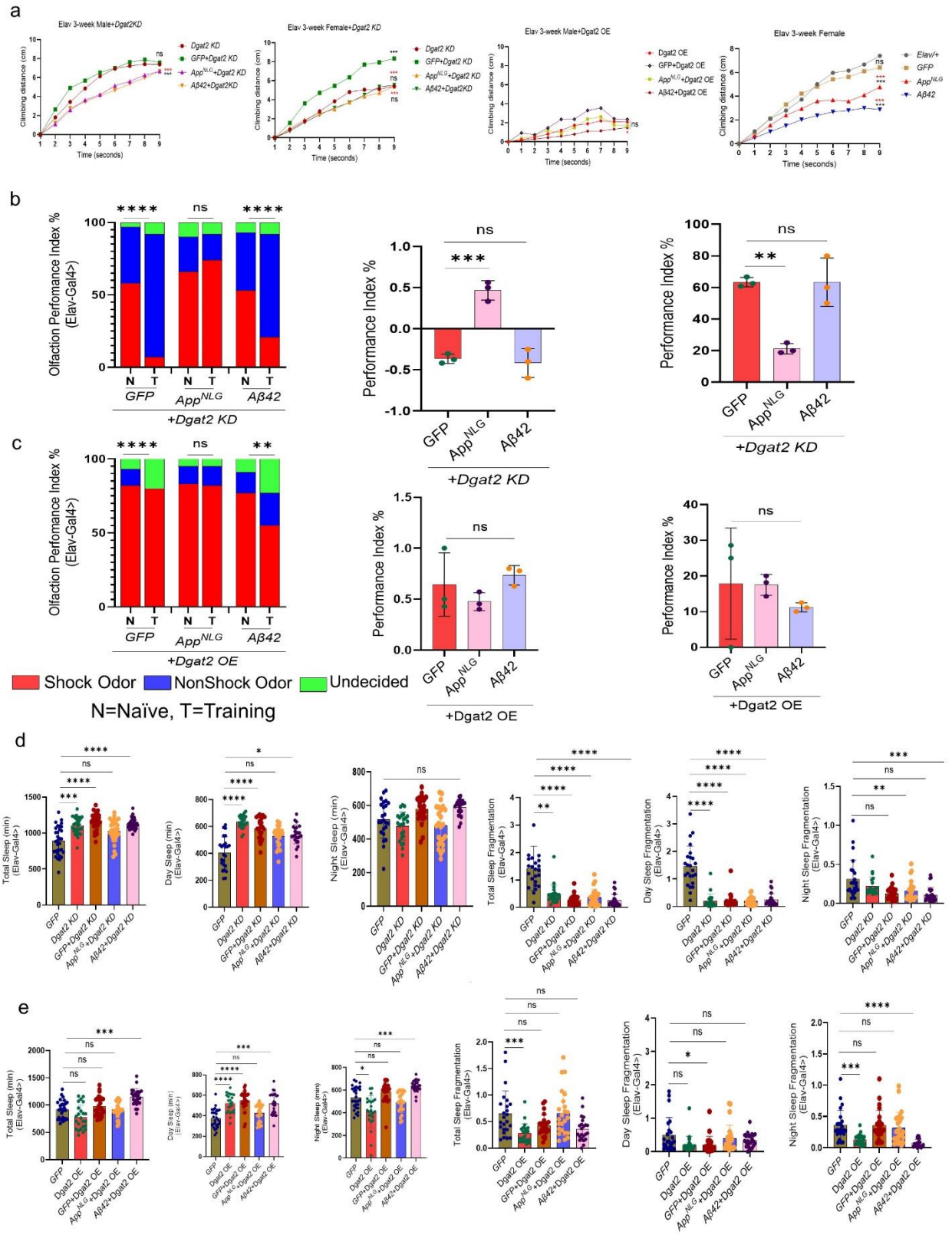
a
Elav 3-week Male+Dgat2KD
Elav 3-week Female+Dgat2 KD
Elav 3-week Male+Dgat2 OE
Elav 3-week Female
Climbing distance (cm)
Time (seconds)
Dgat2 KD
GFP+Dgat2 KD
App^NLG+Dgat2 KD
Aβ42+Dgat2KD
Dgat2 OE
GFP+Dgat2 OE
App^NLG+Dgat2 OE
Aβ42+Dgat2 OE
Elav/+
GFP
App^NLG
Aβ42
b
Olfaction Perfomance Index % (Elav-Gal4>)
N T
GFP
App^NLG
Aβ42
+Dgat2 KD
Performance Index %
c
+Dgat2 OE
Shock Odor
NonShock Odor
Undecided
N=Naïve, T=Training
d
Total Sleep (min) (Elav-Gal4>)
Day Sleep (min) (Elav-Gal4>)
Night Sleep (min) (Elav-Gal4>)
Total Sleep Fragmentation (Elav-Gal4>)
Day Sleep Fragmentation (Elav-Gal4>)
Night Sleep Fragmentation (Elav-Gal4>)
e

Fig.5| *Dgat2 KD* enhances locomotor and cognitive performance, restores sleep activity, and reduces fragmentation linked to *App^{NLG} and Aβ42* expression.

a, Negative geotaxis assay of Elav-driven *Dgat2 KD* and OE in A*pp^{NLG} and Aβ42* models in 3wk male and female (red asterisk denotes significance with *Dgat2 KD+GFP* and/or Dgat2 OE+GFP while black asterisks, ns, denotes significance with *Dgat2 KD* and/ or Dgat2 OE)**. b, (Left panels only),** *Dgat2 KD* overcame deficits in olfactory aversion training in Elav-driven 3-week-old male *App^{NLG} and Aβ42* models. **c, (Left panels only),** Dgat2 OE does not affect deficits in olfactory aversion training in Elav-driven 3-week-old male *App^{NLG} and Aβ42* models; data combined from triplicate assays. Significance was based on the chi-square test. Values are shown as the percentage of flies in each chamber at the end of the assay. **b, (middle panels only),** the difference between fly decisions in Elav-driven *Dgat2 KD* in 3-week-old male *App^{NLG} and Aβ42* models. **c, (middle panels only),** the difference between fly decisions in Elav-driven Dgat2 OE in 3-week-old male *App^{NLG} and Aβ42* models. **b, (right panels only),** flies avoiding shock odor in Elav-driven *Dgat2 KD* in 3-week-old male *App^{NLG} and Aβ42* models. **c, (right panels only),** flies avoiding shock odor in Elav-driven *Dgat2 KD* in 3-week-old male *App^{NLG} and Aβ42* models. **d,** Total, day and night sleep (in minutes) and sleep fragmentation in Elav-driven *Dgat KD* in *App^{NLG} and Aβ42* models. **e,** Total, day and night sleep (in minutes) and sleep fragmentation in Elav-driven Dgat OE in *App^{NLG} and Aβ42* models. Data=mean ± SD. One-way ANOVA with Tukey's multiple comparisons test was performed (**Left and right panels only**). Mixed LM (Linear model) Effects comparisons were performed for geotaxis, n=3 replicates per group and each group had 10 flies. Non-parametric One-way ANOVA with multiple comparisons done with the Kruskal Wallis test was performed for sleep activity and sleep fragmentation. *p<0.05, **p<0.01, and ***p<0.001. n.s = not significant (an asterisk denotes significance for the average of all three replicates). Raw data and *p values* are provided in the source data.

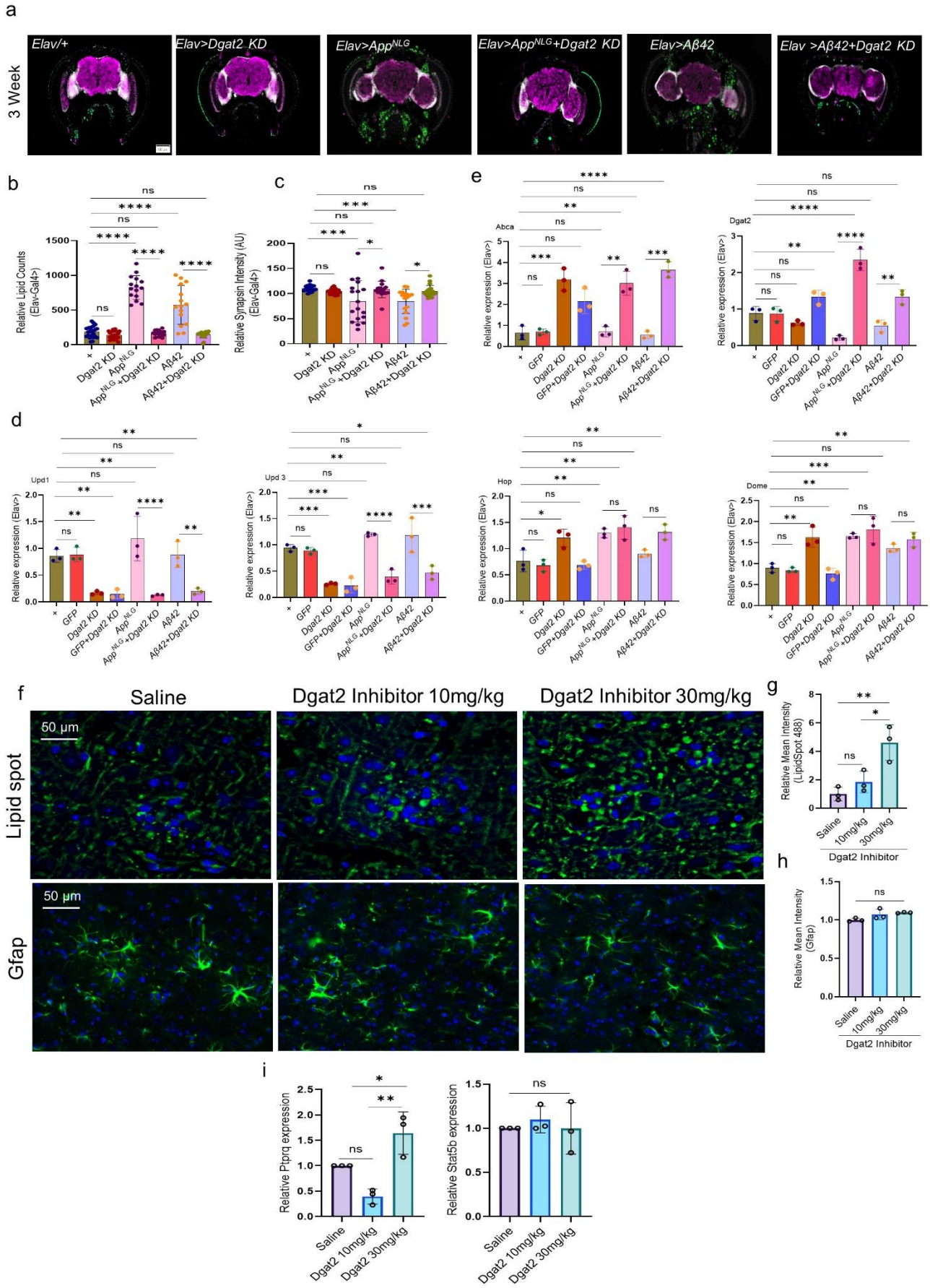
a
3 Week
Elav/+
Elav>Dgat2 KD
Elav>App^NLG
Elav>App^NLG+Dgat2 KD
Elav>Aβ42
Elav >Aβ42+Dgat2 KD
b
Relative Lipid Counts (Elav-Gal4>)
c
Relative Synapsin Intensity (AU) (Elav-Gal4>)
e
Abca
Dgat2
Relative expression (Elav>)
d
Upd1
Upd 3
Hop
Dome
Relative expression (Elav>)
+
GFP
Dgat2 KD
GFP+Dgat2 KD
App^NLG
App^NLG +Dgat2 KD
Aβ42
Aβ42+Dgat2 KD
f
Saline
Dgat2 Inhibitor 10mg/kg
Dgat2 Inhibitor 30mg/kg
Lipid spot
Gfap
50 μm
g
Relative Mean Intensity (LipidSpot 488)
Saline
10mg/kg
30mg/kg
Dgat2 Inhibitor
h
Relative Mean Intensity (Gfap)
i
Relative Ptprq expression
Relative Stat5b expression
Saline
Dgat2 10mg/kg
Dgat2 30mg/kg

Fig.6| *Dgat2 KD* suppresses lipid metabolism, restores synaptic loss, and reduces inflammation in *App^{NLG} and Aβ42* models of *Drosophila*, while Dgat2 inhibition modulates AD risk genes in *App^{NLG-F}* mice. a, Representative image showing the expression of lipid accumulation (green, Lipid spot 488); synaptic loss (purple, anti SYNORF1); a marker of neurodegeneration, and DAPI (white), in the brains of Elav-driven KD in *App^{NLG} and Aβ42* models**. b-c,** Quantification of the expression level of lipid counts and synapsin intensity in Elav-driven *App^{NLG} and Aβ42* models. **d,** Relative expression of inflammatory genes, Upd1, Upd3, Hop and Dome in flies. **e,** Relative expression of metabolic genes, Abca and Dgat2 in flies. **f,** Immunofluorescence staining of lipid spot intensity and Gfap in microglia within the cortex region of the brain of *App^{NLG-F}* mice in the absence and presence of a Dgat2 inhibitor. **g,** Quantification of the Lipid spot intensity, **h,** Quantification of the Gfap immunostaining intensity, n=3 mice per group. **i,** Relative expression level of inflammatory genes in *App^{NLG-F}* mice in the absence and presence of a Dgat2 inhibitor. Data=mean ± SD. One-way ANOVA with Tukey's multiple comparisons test was performed on flies and mouse data. n=3 replicates per group and each group has 8-10 flies. $p < 0.05$; $^{**}p < 0.01$; $^{***}p < 0.001$; ns = not significant (an asterisk denotes significance for the average of all three replicates). Raw data and *p values* are provided in the source data

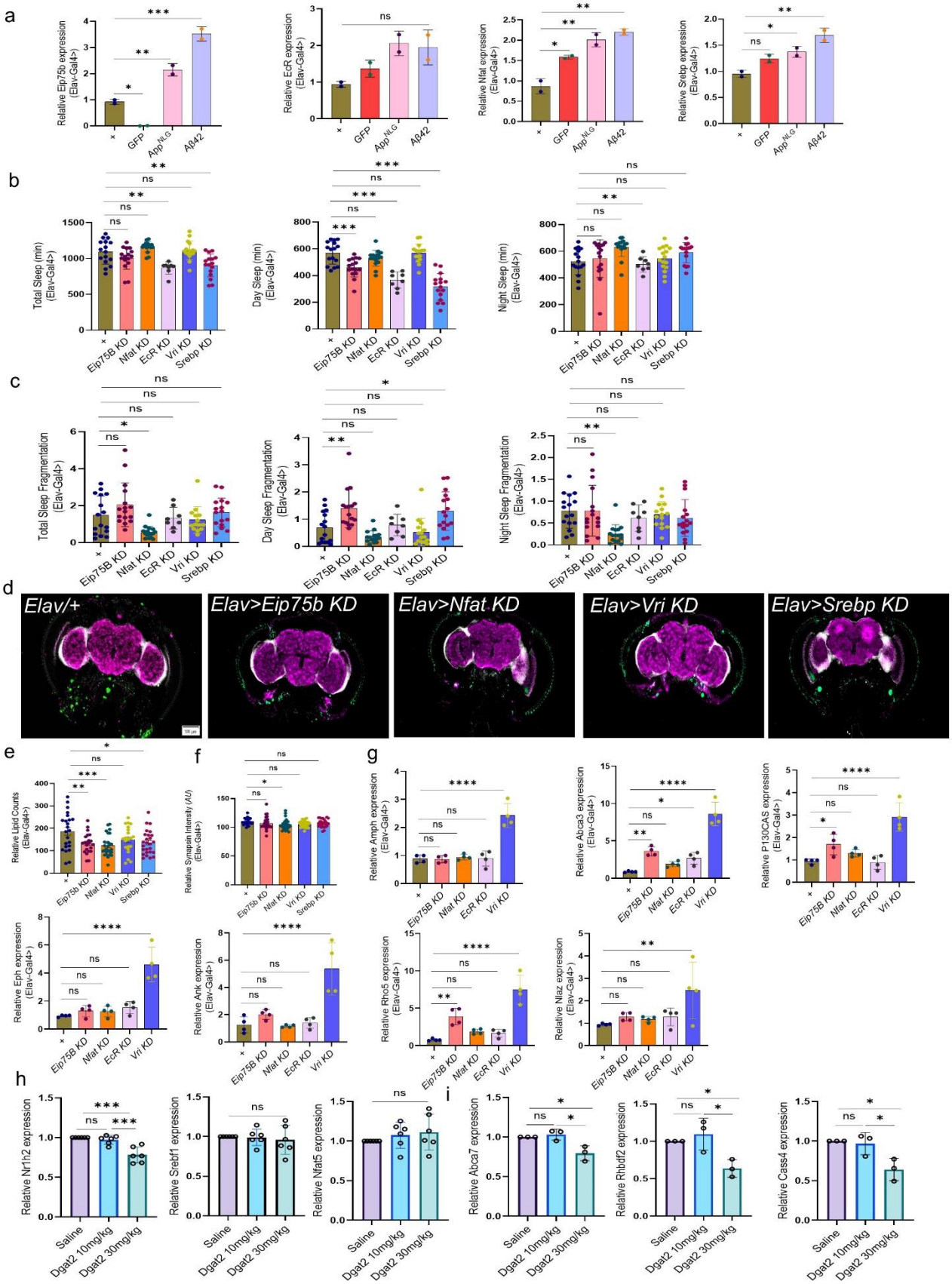
a
Relative Eip75b expression (Elav-Gal4>)
Relative EcR expression (Elav-Gal4>)
Relative Nfat expression (Elav-Gal4>)
Relative Srebp expression (Elav-Gal4>)
+
GFP
App NLG
Aβ42
b
Total Sleep (min) (Elav-Gal4>)
Day Sleep (min) (Elav-Gal4>)
Night Sleep (min) (Elav-Gal4>)
+
Eip75B KD
Nfat KD
EcR KD
Vri KD
Srebp KD
c
Total Sleep Fragmentation (Elav-Gal4>)
Day Sleep Fragmentation (Elav-Gal4>)
Night Sleep Fragmentation (Elav-Gal4>)
d
Elav/+
Elav>Eip75b KD
Elav>Nfat KD
Elav>Vri KD
Elav>Srebp KD
e
Relative Lipid Counts (Elav-Gal4>)
f
Relative Synapsin Intensity (AU) (Elav-Gal4>)
g
Relative Amph expression (Elav-Gal4>)
Relative Abca3 expression (Elav-Gal4>)
Relative P130CAS expression (Elav-Gal4>)
Relative Eph expression (Elav-Gal4>)
Relative Ank expression (Elav-Gal4>)
Relative Rho5 expression (Elav-Gal4>)
Relative Nlaz expression (Elav-Gal4>)
h
Relative Nr1h2 expression
Relative Srebf1 expression
Relative Nfat5 expression
i
Relative Abca7 expression
Relative Rhbdf2 expression
Relative Cass4 expression
Saline
Dgat2 10mg/kg
Dgat2 30mg/kg

Fig.7| Dgat2 transcription factor KD alters sleep activity, reduces lipid accumulation, and modulates AD risk genes in Drosophila, while inhibition of Dgat2 reduced AD risk gene expressions in *App^{NLG-F}* mice. a, Relative Dgat2 transcription factors expressions level in Elav-driven *App^{NLG} and Aβ42*. **b,** Total, day and night sleep (minutes) in Elav-driven Dgat2 TFs KD models. **c,** Total, day and night sleep fragmentation in Elav-driven Dgat2 TFs KD models. **d,** Representative image showing the expression of lipid accumulation (green), synaptic loss (purple), a marker of neurodegeneration, and DAPI (white) in the brains of Elav-driven Dgat2 TFs KD models**. e-f,** Quantification of the expression level of lipid counts **e,** and synapsin intensity **f,** in Elav-driven Dgat2 TFs KD models**. g,** Relative expressions level of AD risk genes, Amph, Abca3, P130CAS, Eph, Ank, Rho5 and Nlaz in Elav-driven Dgat2 TFs KD models. **h**, Relative expressions level of Dgat2 TFs Nr1h2, Srebf1 and Nfat5 in *App^{NLG-F}* mice in response to Dgat2 inhibition. **i,** Relative expression level of AD risk genes, Abca7, Rhbdf2 and Cass4 in *App^{NLG-F}* mice in the presence of Dgat2 inhibitor. Data=mean ± SD. One-way ANOVA with Tukey's multiple comparisons test was performed on flies and mouse data. N=3 replicates per group and each group has 8-10 flies and n=3 mice per group. *$p < 0.05$; **$p < 0.01$; ***$p < 0.001$; ns = not significant (an asterisk denotes significance for the average of all three replicates). Raw data and *p values* are provided in the source data.

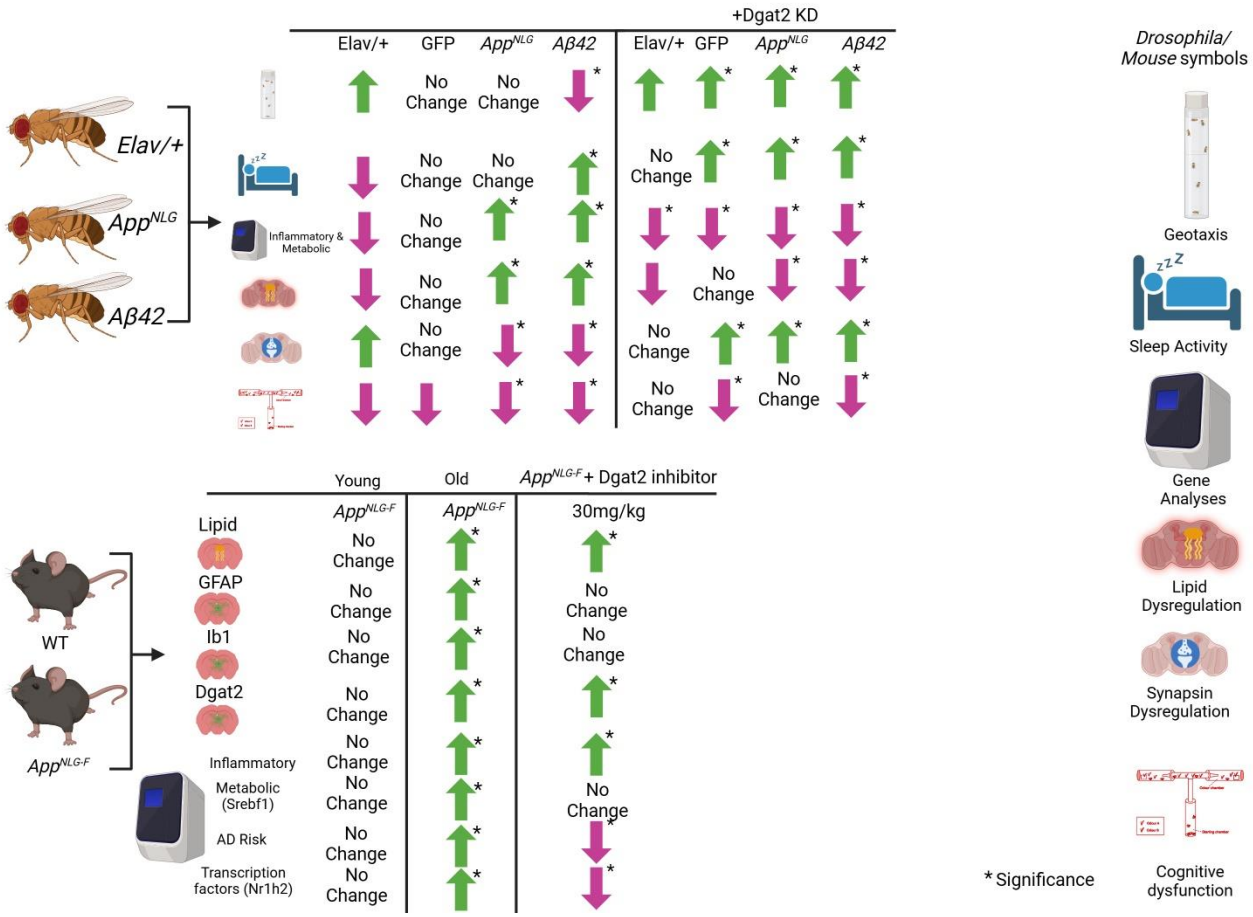

Fig.8. Schematic diagram

Graphical illustration showed the impacts of panneuronal and glial-specific expression of *App^{NLG} and Aβ42* without and with *Dgat2 KD* in Drosophila and microglial/ astrocytic activation and lipid accumulation in *App^{NLG-F}* mice. The top panel result shows that panneuronal and glial-specific expression of *App^{NLG} and Aβ42* led to compromised locomotor and cognitive performance. It also led to enhanced lipid accumulation and reduced synapsin levels, which were further rescued with *Dgat2 KD* (up and down arrows). The bottom panel shows the changes in Gfap, Iba1, Dgat2 stain, inflammatory, and AD risk gene expression in young/old *App^{NLG-F}* mice.